Title

Non-canonical activation of PAR1 induces autophagy in mammalian breast cancer cells

Saibal Saha[a], Rishikesh Kumar[a], Snehanjan Sarangi[b], Rima Tapader[a], Tanusree Ray[c], Animesh Gope[d], Niraj Nag[a], Ananda Pal[d], Amit Pal[a¶]

[a]Division of Molecular Pathophysiology, ICMR-National Institute for Research in Bacterial Infections (ICMR-NIRBI), Kolkata, India; [b]Department of Oral Pathology, Dr. R Ahmed Dental College and Hospital, Kolkata, India; [c]Division of Bacteriology, ICMR-National Institute for Research in Bacterial Infections (ICMR-NIRBI), Kolkata, India; [d]Division of Clinical Medicine, ICMR-National Institute for Research in Bacterial Infections (ICMR-NIRBI), Kolkata, India

[¶]Corresponding author

Key words: HAP; Peptide PAFISED; Peptide PFISED; Mammalian breast cancer; Peptide induced autophagy

Abbreviation

3-MA: 3-Methyladenine

4T1: 410.4 subpopulation Tumor 1

AL: Autolysosome

AMPK: Adenosine 5′-monophosphate-activated protein kinase

AP: Autophagosome

Atg: Autophagy related protein

BECN1: Beclin 1

DAPI: 4',6-diamidino-2-phenylindole

EAC: Ehrlich ascites carcinoma

EDTA: Ethylenediamine tetraacetic acid

ERK1/2: Extracellular signal-regulated protein kinase 1/2

FBS: Fetal bovine serum

FIP200: Focal adhesion kinase family-interacting protein of 200 kDa

FITC: Fluorescein isothiocyanate

GABARAP: Gamma-aminobutyric acid receptor-associated protein

GAPDH: Glyceraldehyde-3-phosphate dehydrogenase

GATE-16: Golgi-associated ATPase enhancer of 16 kDa

GFP: Green fluorescence protein

HAP: Hemagglutinin protease

HRP: Horseradish peroxidase

IgG: Immunoglobulin G

JNK: Jun N-terminal kinase

KD: Knocked down

Ki-67: Antigen kiel-67

LAMP1: Lysosome associated membrane protein 1

LC3I: Microtubule-associated protein light chain 3 I

LC3II: Microtubule-associated protein light chain 3 II

MAP kinase: Mitogen activated protein kinase

MCF10A: Michigan cancer foundation-10A

MCF7: Michigan cancer foundation-7

MEM: Minimum essential medium

MFI: Mean fluorescence intensity

mTOR: Mammalian target of rapamycin

MTT: 3-(4,5-dimethylthiazol-2-yl)-2,5-diphenyltetrazolium bromide

PAR1: Protease activated receptor 1

PARs: Protease activated receptors

RFP: Red fluorescence protein

RPM: Rotation per minute

RPMI 1640: Roswell park memorial institute 1640

SDS-PAGE: Sodium dodecyl sulfate-polyacrylamide gel electrophoresis

siRNA: Small interfering ribonucleic acid

SQSTM1/p62: Sequestome 1

TBS: Tris-buffered saline

TBST: Tris-buffered saline Tween-20

TEM: Transmission electron microscope

ULK1: Unc-51-like kinase 1

VPS15: Vacuolar Protein Sorting 15

VPS34: Vacuolar Protein Sorting 34

WT: Wild type

Abstract

The question of whether autophagy is a boon or a bane for the body does not lend itself to a straightforward answer, as its consequences are intricately tied to the pathophysiological context that triggers its activation. The intricate nature of autophagy's effects on the body, compounded by its multifaceted regulation through various upstream signaling pathways, warrants a deeper and more nuanced research. This study delves into the regulation of autophagy through the non-canonical activation of protease activated receptor 1 (hereafter, termed as PAR1) by Hemagglutinin protease (hereafter, referred as HAP). In contrast to the canonical activation of PAR1 by thrombin, which promotes cell proliferation via the upregulation of mTOR signaling, HAP-induced, non-canonical activation of PAR1 triggers autophagy by downregulating mTOR activation and modulating subsequent key signaling pathways in mammalian breast cancer cells. This non-canonical activation results in the generation of a new N-terminal sequence of PAR1. Moreover, synthetic peptide designed to replicate this newly generated N-terminal sequence effectively triggers autophagy in mammalian breast cancer cells, thereby establishing that induction of autophagy via non-canonical PAR1 activation is independent of the activating agent of PAR1 itself. The study also explores the implications of peptide-induced autophagy in the context of early-stage, low-grade breast cancer using a BALB/c mouse model, demonstrating substantial inhibition of tumor growth and a delay in carcinogenesis progression. Importantly, the absence of notable PAR1 expression in normal, healthy cells ensures that they remain unaffected by the peptide, positioning it as a promising candidate for targeted therapy in low-grade breast cancer.

Introduction

The literal meaning of ‘autophagy’ as derived from its Greek origin (Greek word ‘Auto’ means ‘Self’ and ‘Phagos’ means eat) [1] does not fully encapsulate its multifaceted roles across various cellular contexts. Beyond its cytoprotective functions, macroautophagy (hereafter referred as autophagy) can also lead to a specific form of cellular death known as type II programmed cell death. Autophagy is an evolutionarily conserved adaptive response of cell initiated by a number of external and internal stimuli [2, 3]. Generally, cells recruit autophagy as a sophisticated recycling mechanism in which dysfunctional or superfluous organelles, invading pathogens, or non-essential organelles under stressed condition are enclosed within a double-membrane vesicle termed as phagophore, resulting in the formation of autophagosome (hereafter referred as AP). Although, in autophagy, the selection of the substrate for autophagic degradation is majorly random (bulk degradation), evidences are not scarce for selective degradation [4-7]. SQSTM1/p62 and NBR1 act as adapter molecules for the transportation of the selected ubiquitinated molecules to the phagophore [8-10]. Once AP formation is complete, it subsequently fuses with lysosome to form autolysosome (hereafter referred as AL), culminating to the degradation of the sequestered components through proteolytic activity of lysosomal hydrolases and the building blocks are released to the cytosol for further utilization [11]. Recent developments on autophagy research have also shed light on the events of incomplete autophagy where various stimuli initiate the process of phagophore formation and sequestration but fail to further proceed to the fusion of AP and lysosome resulting into accumulation of cargo [12]. Impaired autophagy is also implicated in several neurodegenerative disorders including Alzheimer and Parkinson diseases, cancers, autoimmune diseases, metabolic syndromes including type 2 diabetes, cardiovascular and

pulmonary disorders, reproductive dysfunctions, ocular disorders including age related macular degeneration, musculoskeletal diseases including degenerative myopathies, hepatic disorders and renal diseases [13].

In cancer, autophagy plays a complex, dual role that varies with the disease stage. In the early stages of cancer, autophagy acts as a tumor-suppressive mechanism by degrading misfolded proteins and pathogens, potentially preventing further tumor development. Conversely, in later stages, cancer cells exploit autophagy to survive and adapt to the hostile environment created by the host [14-17].

Proteases are pivotal in the autophagic process. The interplay between proteasomal degradation and autophagy serves as a compensatory mechanism for the breakdown of various cellular components; an obstruction in one pathway often augments the other. For instance, inhibition of 26S proteasome leads to the activation of AMPK [18-20], a positive regulator of autophagy [21]. Nevertheless, certain proteases facilitate the induction of autophagy. Notably, a cysteine protease HsApg4A cleaves the C-terminal end of the three mammalian homologs of Atg8 (GABARAP, LC3 and GATE-16), thereby promoting the formation of autophagic vacuoles [22, 23]. However, numerous studies indicate that bacterial proteases can inactivate the autophagy machinery, enabling bacteria to evade autolysosomal degradation. For example, the protease RavZ, produced by *L. pneumophila* functionally mimics Atg4B-like cysteine protease and impedes the formation of AP by dissociating LC3 from phosphatidylethanolamine[24]. Proteases can trigger various signaling pathways by interacting with protease activated receptors (hereafter referred as PARs), which include four subtypes (PAR1 to PAR4) [25]. Among these G-protein coupled receptors, expression of PAR1, PAR2 and PAR4 is significantly higher in cancer cells than in normal cells, making them promising targets for cancer therapy [26]. Thrombin acts as a typical activator of PARs by making a proteolytic cleavage at N-terminal extracellular region of PARs and the N-

terminal region acts as a tethered ligand that binds to the second extracellular loop of the receptor. This thrombin mediated activation of PAR1 upregulates the phosphorylation of mTOR [27], which is a master regulator of autophagy [28, 29]. Hence, it not only results into activation of coagulation cascades but also leads to several other cellular events, which includes induction of angiogenesis and promotion of growth and proliferation of metastatic cancer cells [30].

HAP, a 35 kDa zinc-dependent secretory metalloprotease, isolated from *Vibrio cholerae* O1 strain (C6709), has been reported to induce apoptosis in mammalian breast cancer cells [31]. Among the four subtypes of PARs, HAP specifically engages with PAR1, facilitating its activation through proteolytic cleavage at the N-terminal region. In Ehrlich ascites carcinoma (EAC) cells, a murine breast cancer cell line, this cleavage creates a new N-terminal extracellular segment, sequenced as PFISEDASGY. Albeit, the precise region of this newly formed N-terminal end, that functions as a tethered ligand and binds intramolecularly to the receptor to initiate downstream signaling pathways, remains unidentified [32]. Subsequently, based on the sequence of the HAP-mediated cleavage site of PAR1 in EAC cells, a peptide (PFISED) was designed, which demonstrated its ability to induce apoptosis in both breast and colon cancer cell lines [33].

Evidently, autophagy being an early response of cell and apoptosis being a late one [34], they share some common upstream signaling pathways, allowing a single stimulus to activate both the processes [35-37]. The current study explored the potential of HAP mediated alternative activation of PAR1 to induce autophagy in mammalian breast cancer cells in a dose- and time-dependent manner.

Results

Hemagglutinin Protease (HAP) induced autophagy

An immunoblot analysis was conducted probing two markers of autophagy, LC3II and LAMP1, revealing a dose- and time-dependent increase of expression in human epithelial breast cancer cells (MCF7, Estrogen receptor+) and murine epithelial breast cancer cells (4T1, Estrogen receptor-) when treated with varying dosages of HAP (ranging from 0.25 µg/ml to 1 µg/ml) for the duration of 30 and 60 mins (Fig. 1 Ai). Densitometric analyses of the immunoblots indicated that the most pronounced and consistent expression of both molecules occurred at a dose of 0.5 µg/ml for MCF7 and 0.75 µg/ml for 4T1 when treated with HAP for 30 mins. At the specified dosage and duration of HAP treatment, LC3II and LAMP1 exhibited significant increases in expression levels in MCF7 cells, with LC3II showing more than a 3-fold increase and LAMP1 over a 22-fold increase compared to controls. In 4T1 cells, LC3II and LAMP1 expression increased approximately by 5-fold and 1.5-fold, respectively, compared to controls. Following 60 mins of HAP treatment, 4T1 cells demonstrated the highest expression levels of both markers at a dose of 0.5 µg/ml, while MCF7 cells displayed peak expression of the two markers at different doses: LAMP1 at 0.25 µg/ml and LC3II at 0.5 µg/ml (Fig. 1 Aii). To ensure uniformity of maximum expression levels of both the molecules in subsequent experiments, we standardized the HAP dosages to 0.5 µg/ml for MCF7 cells and 0.75 µg/ml for 4T1 cells, administered over a 30 mins duration.

Previous studies have reported that higher doses of HAP induce apoptosis in EAC and RAW 264.7 cells (1 µg/ml for EAC and 1 µg/ml & 1.5 µg/ml for RAW 264.7 cells) over a longer

period (2 h) [31]. Our findings suggest that HAP has the potential to induce autophagy in mammalian epithelial breast cancer cells (MCF7 and 4T1) at lower doses and shorter durations.

Further confirmation of autophagy induction in HAP-treated MCF7 and 4T1 cells was achieved using LysoTracker™ and Autophagy detection kit (abcam). LysoTracker™ is a dye that specifically stains lysosomal vacuoles, while the Autophagy detection kit detects autophagosomal as well as autolysosomal vacuoles. Immunofluorescence imaging of LysoTracker™ stained cells revealed an increase in mean fluorescence intensity per cell (MFI per cell) in both MCF7 and 4T1 cells treated with the previously optimised dosages of HAP for 30 mins compared to untreated cells (control). However, pretreatment of cells with Bafilomycin A1, a lysosomal inhibitor, showed no significant increase in the number of lysosomes (Fig. 1 Bi and Bii) upon HAP treatment.

Immunofluorescence imaging using the Autophagy detection kit (Abcam, ab139484) further supported the role of HAP in inducing autophagy in MCF7 and 4T1 cells, indicated a 13-fold and 3.6-fold increase of MFI in MCF7 and 4T1 cells respectively under the previously standardized conditions of HAP treatment compared to their respective control. As per the kit protocol, a positive control was established by co-treating cells with 500 nM rapamycin (an autophagy inducer) and 60 μM chloroquine for 24 h (Fig. 1 Ci and Cii). We have also confirmed this result by flowcytometric analyses of HAP treated MCF7 and 4T1 cells using the Autophagy detection kit (Fig. S1 Ai). Quantitative analyses showed significantly elevated MFI in the HAP treated cells (Fig. S1 Aii).

Additionally, analysis of cathepsin L expression by immunofluorescence imaging confirmed the ablation of autolysosomal membrane in HAP-treated MCF7 and 4T1 cells at the specified dosages and time. Cathepsins are lysosomal enzymes that facilitate the degradation of

autophagy substrates in the final stages of autophagy. Among these enzymes, cathepsin L degrades the lysosomal membrane and is released into the cytosol after the disruption of autolysosomal vacuoles [38]. Immunofluorescence imaging revealed significantly higher expression of cathepsin L in HAP-treated MCF7 and 4T1 cells under the previously optimised conditions compared to control. Notably, upon pretreatment with the autophagy inhibitor 3-Methyladenine (3-MA), HAP treatment could not lead to a significant increase in cathepsin L expression (Fig. 1 Di and Dii).

Role of PAR1 in HAP-induced autophagy

In this study, we probed the expression of PAR1 in MCF7 and 4T1 cells following treatment with HAP at dosages ranging from 0.25 μg/ml to 1 μg/ml for 30 and 60 mins. In MCF7 cells, a notable increase in PAR1 expression was observed at doses of 0.5 and 0.75 μg/ml after 30 mins and at 0.25 and 0.5 μg/ml after 60 mins. Similarly, in 4T1 cells, most upregulated expression was found at 0.75 μg/ml after 30 mins and at 0.25 and 0.5 μg/ml after 60 mins (Fig. 2 Ai and Aii). These dosages of HAP that induced PAR1 upregulation are consistent with the previously optimized dosages for autophagy induction, leading to speculation of a plausible role of PAR1 in HAP-induced autophagy in MCF7 and 4T1 cells. To evaluate the interaction between HAP and PAR1, we assessed the colocalization of HAP and PAR1 using confocal microscope in both MCF7 and 4T1 cells treated with the specific doses of HAP optimized for autophagic induction (0.5 μg/ml and 0.75 μg/ml doses of HAP respectively in MCF7 and 4T1 for 30 mins). Immunofluorescence imaging using HAP anti-sera and PAR1 antibody revealed significant co-localization of HAP and PAR1 in MCF7 and 4T1 cells compared to controls (Fig. 2 Bi), confirming the interaction between HAP and PAR1. Co-localization was quantified in term of Pearson's correlation coefficient, which indicated a three-times and 1.7-times increase in the HAP treated MCF7 and 4T1 cells respectively compared to their respective untreated control (Fig 2 Bii).

To investigate the role of PAR1 in HAP-induced autophagy, we transiently knocked down PAR1 in MCF7 cells using small interfering ribonucleic acid (siRNA) (CGGUCUGUUAUGUGUCUAUdTdT) (Fig. 2 Ci and Cii), followed by treatment with HAP (0.5 μg/ml for 30 mins and 0.25 μg/ml for 60 mins). SQSTM1/p62, which acts as a scavenger of the cargo for their autophagic degradation, binds to LC3 and is degraded within the AL [9]. Thus, decreased level of SQSTM1/p62 marks the cargo sequestration inside the AL. Immunoblotting for LC3II and SQSTM1/p62 in wild type (WT) and PAR1 knocked down (PAR1 KD) MCF7 cells treated with HAP revealed a substantial reduction in SQSTM1/p62 and an increase in LC3II in HAP treated WT cells. However, changes in these markers were minimal in PAR1 KD cells treated with HAP (Fig. 2 Di). Densitometric analyses showed a 3.7-fold and 6.1-fold decrease in SQSTM1/p62, and a 2.1-fold and 1.75-fold increase in LC3II in WT MCF7 cells treated with 0.5 μg/ml of HAP for 30 mins and 0.25 μg/ml for 60 mins, respectively. In contrast, no statistically significant change was observed in SQSTM1/p62 and LC3II expression in PAR1 KD MCF7 cells treated with HAP (Fig. 2 Dii).

Further evidence for PAR1's involvement in HAP-induced autophagy was provided by flow cytometric analyses using LysoTracker™ staining of WT and PAR1 KD MCF7 cells treated with various dosages of HAP for 30 and 60 mins (Fig. 2 Ei). LysoTracker™ fluorescence falls in the excitation-emission range of FITC. Flow cytometry indicated a 10-fold increase in percentage of FITC-positive cells in WT MCF7 cells treated with 0.5 and 0.75 μg/ml HAP for 30 mins, and a 9.4-fold and 8.4-fold increase with 0.25 and 0.5 μg/ml HAP for 60 mins compared to control cells. There was no significant increase in percentage of FITC-positive cells in PAR1 KD MCF7 cells treated with 0.5 μg/ml HAP for 30 mins and 0.25 and 0.5 μg/ml HAP for 60 mins. Nevertheless, PAR1 KD cells treated with 0.75 μg/ml HAP showed a

significant, albeit minimal, increase in FITC-positive cells, approximately threefold compared to control cells (Fig. 2 Eii).

in silico analyses of the interaction between PAR1 and the peptides

Earlier, our lab has reported the interaction between PAR-1 and the cleaved N-terminal sequence of PAR-1, PFISED (generated by the HAP mediated cleavage of PAR-1) as a tethered ligand in murine breast cancer cells as the underlying mechanism of HAP induced apoptosis. However, the interaction between the human homolog of PAR-1 and the it's N-terminal amino acid sequence at the similar position (PAFISED) has not yet investigated. So, we have analyzed the interaction between human as well mouse homolog of PAR-1 with the peptides PAFISED and PFISED respectively with the help of bioinformatics tools.

Molecular Docking is a computational method to predict the non-covalent bonds between macromolecules (receptors) and smaller molecules (ligands) with more reliability and efficiency. Ideally, the binding affinity and conformation of the bound molecules need to be predicted. The physico-chemical properties like drug-likeness properties, pharmacokinetics, and toxicity of the peptides were checked before docking (Table. S1). 3D structures of peptides were predicted and top pose then used as a ligand in Autodock Vina (Fig S2 A). The native ligand vorapaxar interactions suggest that Val 257, Tyr 337, Leu 258 and Ala 349 are important for protein-ligand complex (Fig. 3A). The re-docked vorapaxar parameters were used for Autodock Vina to perform docking and then we used CABS-dock for the blind docking (Fig. 3 B). The binding affinity of the of peptide PAFISED and PFISED were examined with PAR1. The re-docked Vorapaxar has shown -13.136 kcal/mol of binding affinity with Tyr 337 and Val 257 hydrogen interactions with the PAR1 while the peptides PAFISED and PFISED has -6.721 kcal/mol and -5.160 kcal/mol binding affinity respectively as analyzed by Autodock Vina (Fig. 3 B and PAFISED has hydrogen interaction like Tyr-

337, Leu-263 and Thr-261 but PFISED has only Tyr 337, Tyr 95, Tyr 350, Tyr 187 hydrogen interaction in top most docking pose (Fig. 3 B, Ci and Cii). The Blinding docking was also performed and both peptide shows good interaction with PAR-1. The cluster density of PAFISED and PFISED were 16.34 & 29.33, average RMSD 7.40 & 2.86, max RMSD 32.88 & 28.90 with number of elements in selected cluster 121 & 84 respectively (Fig S2 C and D). The hydrogen bond interaction (Table S2) and hydrophobicity (Fig S2 B) of top docked pose by CABS dock were also analysed by Biovia Discovery Studio visualizer.

Induction of autophagy is regulated by an alternative activation of PAR1 by HAP

To compare thrombin mediated conventional activation of PAR1 with the alternative PAR1 activation by HAP in respect of their potential to induce autophagy, we analyzed two markers of autophagy, LC3II and LAMP1 in MCF7 and 4T1 cells by immunoblotting. Densitometric analyses of the immunoblots revealed no significant upregulation of any of the markers in thrombin-treated cells compared to controls. In contrast, HAP-treated MCF7 cells showed a 16.8-fold increase in LC3II and a 6.6-fold increase in LAMP1, while 4T1 cells exhibited an 8.65-fold increase in LC3II and nearly a threefold increase in LAMP1. Additionally, we assessed phospho-mTOR (Ser 2448) and total mTOR expression in both thrombin and HAP-treated cells. HAP treatment resulted in a 4.2-fold and 6.8-fold downregulation of phospho-mTOR in MCF7 and 4T1 cells, respectively, consistent with the notion that mTOR activation negatively regulates autophagy. However, the increase in mTOR phosphorylation in either of the thrombin treated cells was statistically insignificant (Fig 4 Ai and Aii).

In EAC cells, HAP-mediated cleavage of PAR1 exposes the sequence PFISED, which binds PAR1 as a tethered ligand [33]. The human PAR1 homolog (UniProt ID: P25116) has the similar sequence, at the identical position at the N-terminal end with addition of one alanine residue in between proline and phenylalanine (PAFISED), which has been shown here

bioinformatically to bind with PAR1 intramolecularly. Given that the synthetic hexapeptide SFLLRN mimics thrombin's effect on PAR1 without requiring proteolytic cleavage of PAR1 by thrombin [39], we evaluated the autophagic potential of synthetic peptides PFAISED in comparison to SFLLRN in MCF7 cells by immunoblotting SQSTM1/p62. The identical position of mouse PAR1 homolog has a sequence SFFLRN. So, we have compared their ability to induce autophagy by probing the same marker. Additionally, a scramble peptide (HTPPPPFISEDASGY) was included to further assess the specificity of the peptide (PAFISED and PFISED) to induce autophagy (Fig. 4 Bi). Quantitative analyses revealed a fourfold decrease in SQSTM1/p62 expression in PFAISED-treated cells relative to control. In contrast, no significant change in SQSTM1/p62 expression was observed in SFLLRN or scramble peptide-treated cells (Fig. 4 Bii).

Potential of the synthetically designed peptides to induce autophagy

Based on the cleavage site of Protease Activated Receptor-1 (PAR1) by HAP, we synthesized two peptides that emulate the newly generated N-terminal end of PAR1 following HAP-mediated cleavage in human and murine epithelial cancer cells. The capacity of these peptides to induce autophagy was evaluated in a dose-dependent manner, ranging from 5 to 100 μM, using human (MCF7) and murine (4T1) breast epithelial cancer cell lines. This was accomplished by immunoblotting for autophagy markers, specifically LC3, LAMP1, and SQSTM1/p62 (Fig. 4 Ci).

The optimal concentrations identified for autophagy induction were 50 μM for the PFAISED peptide and 75 μM for the PFISED peptide in MCF7 and 4T1 cells, respectively. Densitometric analyses of the immunoblots at these concentrations revealed a 2.47-fold increase in the LC3II/LC3I ratio and a 3.35-fold increase in LAMP1 expression in MCF7 cells. In 4T1 cells, the increases were 2.52-fold for LC3II/LC3I and 3.23-fold for LAMP1.

Additionally, SQSTM1/p62 expression decreased by 4.4-fold in MCF7 cells and 2.76-fold in 4T1 cells (Fig. 4 Cii).

The induction of autophagy by these peptides was further confirmed using a confocal microscopy approach with the Autophagy detection kit (Abcam, ab139484). Significant increases in green puncta, indicative of autophagosomal and autolysosomal vacuoles, were observed in MCF7 and 4T1 cells treated with PFAISED (50 μM) and PFISED (75 μM), respectively, compared to control cells. Cells treated with both rapamycin (500 nM) and chloroquine (60 μM) for 24 h served as positive controls (Fig. 4 Di). Quantitative analyses of confocal images demonstrated an approximately 12-fold increase in mean fluorescence intensity per cell in MCF7 cells treated with the PFAISED peptide, while the increase in 4T1 cells treated with the PFISED peptide exceeded 13-fold compared to their respective controls (Fig. 4 Dii). These finding were further corroborated by flowcytometric analyses of the peptide treated cells using the Autophagy detection kit (Figure S1 Ai), which upon quantification showed a significant increase of MFI in the peptide treated cells compared to the respective controls (Fig. S1 Aii).

We have also evaluated the effect of HAP and the peptide PFAISED on normal breast epithelial cells MCF-10A in aspect of induction of autophagy by probing the autophagy markers LAMP1 and LC3 along with PAR1. Immunoblots revealed a negligible expression of PAR1 in MCF-10A compared to MCF7. We also could not find any visible expression of either LAMP1 or LC3 in MCF-10A (Fig. S3 C).

Signaling pathway of peptide induced autophagy

Once the autophagy-inducing potential of the peptide was established, we delved deeper into the underlying signaling pathway. ULK1, a serine/threonine protein kinase, serves as a critical component in the assembly of the autophagy initiation complex [40]. It is noteworthy

that AMPK and mTOR compete to each other for the phosphorylation of ULK1. The activated mTOR (p-mTOR) phosphorylates ULK1 at the Ser757 position, preventing its interaction with ATG101, ATG13, and FIP200, which are essential for the formation of this complex. Conversely, AMPK facilitates the assembly of the initiation complex. Upon activation, AMPK phosphorylates ULK1 at Ser 317 and Ser 777, distinct sites from that phosphorylated by mTOR [21].

In our study, we assessed the activation status of mTOR and AMPK in MCF7 cells treated with varying concentrations of the peptide PFAISED through immunoblotting. Notably, treatment with 50 µM of the peptide led to a significant 16.21-fold reduction in p-mTOR levels, while p-AMPK (the activated form) levels exhibited a substantial increase of approximately 6.5-fold compared to control cells. Furthermore, immunoblot analyses of ULK1 phosphorylation revealed a 1.5-fold decrease in p-ULK1^{Ser757} and a 2.86-fold increase in p-ULK1^{Ser317} under the same experimental conditions. Following the formation of the initiation complex, Beclin1 is recruited to form the BECN1-VPS34-VPS15 core complex, which is instrumental in the nucleation phase of autophagy. Densitometric analyses of the immunoblot revealed a 3.46-fold increase in BECN1 expression in cells treated with the optimized dosage of PFAISED (Fig. 4 Ei and Eii). We have further probed the phosphorylation of the three MAP kinases *viz*. ERK1/2, p38 and JNK to have a better insight of the molecular mechanism lying behind mTOR downregulation by the peptide (Fig. 4 Fi). Densitometric analyses of the immunoblots indicated a more than 4-fold downregulation in the phosphorylation of ERK1/2 and JNK, while phophosrylation of p38 has shown approximately 2-fold decrease in MCF7 cells treated with 50 µM dosage of peptide PAFISED compared to the untreated control (Fig. 4 Fii).

Potential of HAP and the peptides to form AL

To facilitate autophagy-mediated cell death, it is imperative that the autophagosomal structure successfully fuses with the lysosome to form an AL. Numerous autophagy-inducing agents, such as chloroquine, are unable to advance this process to completion, particularly, the maturation of AP into AL, along with the subsequent degradation of cargo. Therefore, assessing the ability of either HAP or the peptides to induce the formation of ALs is fundamental for the evaluation of autophagy-mediated cell death.

To investigate the fusion of AP with lysosome, we employed a plasmid construct, pMXs GFP-LC3-RFP, as an autophagy flux reporter. Following the transfection of the cells with this plasmid construct, endogenous ATG4 family proteins cleave it to yield equimolar amounts of GFP-tagged LC3 and RFP. Upon fusion of the AP with the lysosome, GFP-tagged LC3 is delivered into the lysosomal compartment along with other cargo, where the acidic environment quenches its fluorescence. In contrast, RFP remains in the cytosol and exhibit normal fluorescence as its fluorescence is pH-independent. Consequently, a decreased GFP:RFP ratio is observed which serves as an indicator of autophagy flux [41]. After transfecting MCF7 and 4T1 cells with the plasmid, we treated them with previously optimized dosages of HAP and the peptides. Confocal microscopy analyses revealed a reduced GFP:RFP ratio in the treated cells (Fig. 5 Ai). HAP treatment led to a greater than 3-fold increase in RFP:GFP ratio in MCF7 cells, whereas, in 4T1 cells, the increase was observed to be over 5-fold. Treatment with the peptide PFAISED resulted in a substantial more than 8-fold increase in the RFP:GFP ratio in MCF7 cells. In contrast, the increase in 4T1 cells treated with the peptide PFISED was more modest, approximately 3-fold (Fig. 5 Aii).

To further corroborate our findings, we examined the colocalization of LC3 and LAMP1 in the peptide-treated MCF7 and 4T1 cells using confocal microscope (Fig. 5 Bi). Given that LC3 is present on both the inner and outer membranes of the AP and LAMP1 is localized to

the lysosomal membrane [42], the colocalization of these two proteins marks the fusion of AP with lysosome. Analyses of the confocal microscope images unfolded a 15.5-fold and 4.7-fold increase in the Pearson's correlation coefficient for colocalization in peptide-treated MCF7 and 4T1 cells, respectively, compared to their respective controls (Fig. 5 Bii).

The formation of ALs was finally confirmed through transmission electron microscopy (TEM) of HAP and peptide-treated MCF7 and 4T1 cells (Fig. 5 C). Ultramicrotome images of the cells using TEM clearly illustrated autolysomal structures characterized by multiple dark patches, indicative of degraded cargo. Although, in HAP and peptide-treated 4T1 cells, we also observed some autophagosomal structures containing intact cellular organelles.

Cancer stage determination of breast tumors developed with 4T1 cells in BALB/c mice

The impact of peptide-induced autophagy on breast cancer cells, as evidenced through *in vitro* analyses, was further substantiated *in vivo* using a BALB/c mouse breast tumor model established by injecting 4T1 cells. Histopathological evaluation of tumors collected at weekly intervals over a six-week period following injection of the 4T1 cells revealed distinct gradations of malignancy. Tumors from weeks 1 to 3 exhibited characteristics of well-differentiated, low-grade (Grade I) cancer, indicative of the early stage of the disease, while tumors from weeks 4 to 6 were moderately differentiated (Grade II), reflecting an intermediate stage of breast cancer (Fig. S4 D and Table S3). Tumor grading adhered to the Nottingham Grading System [43] and correlated to Antigen kiel-67 (Ki-67) expression level.

Tumor volume measurements showed a significant increase at the 5- and 6-week marks (Fig. S4 Ci and Cii), correlating with the histopathologically determined tumor grades. Immunohistochemical analysis of Ki-67 expression, performed at six different time points, revealed a substantial increase in Ki-67 expression in tumors from weeks 4 to 6 compared to those from weeks 1 to 3 (Fig. S4 Ei and Eii), further corroborating the histopathological

findings. Although the mice exhibited a modest, non-significant decrease in body weight up to the third week, a slight increase was noted by the fourth week. Notably, body weight significantly increased during the fifth and sixth weeks, plausibly due to the remarkable increase of the tumor volume (Fig. S4 B).

Peptide-induced autophagy improved survival rate of BALB/c mice carrying low grade solid breast tumors developed with 4T1 cells

Mice with 2-week-old tumors were selected as the early-stage breast cancer model for subsequent experiments. Upon monitoring the survival of the experimental mice, we found an average survival time of around 45 days in the tumor bearing mice, whether the time substantially increased to an average of almost 96 days when treated with the peptide PFISED. Notably, when treated with both the peptide and the autophagy inhibitor, 3-MA, the survival time again declined to an average of approximately 54 days. Mice without tumors demonstrated a significantly longer average survival of around 172 days (Fig. 6B)**.**

Inhibition of tumor growth, progression and proliferation of tumor cells by the peptide induced autophagy at early stage of breast cancer in BALB/c mice

Tumor volume measurements, taken four weeks after the injection of 4T1 cells revealed a statistically significant 47 times lesser volume in the set of tumor-bearing mice those were treated with the peptide PFISED at an interval of 3 days from the 2nd week onward. Remarkably, the tumor bearing mice, those were treated with peptide along with the autophagy inhibitor, 3-MA showed no significant reduction of tumor volume (Fig. 6 Ci and Cii).

Histopathological analyses-based gradation (following the Nottingham grading system) of the tumors, harvested after 4 weeks of 4T1 injection from the three sets of experimental mice, *viz*. tumor bearing mice without any further treatment (tumor control), tumor bearing mice

treated with peptide PFISED and tumor bearing mice treated with the peptide along with the autophagy inhibitor, 3-MA confirmed their grade of malignancy as intermediate-grade (II), low-grade (I) and intermediate-grade (II) respectively (Fig. 6 D and Table 1).

Immunohistochemical analysis of Ki-67 expression in the aforementioned three sets of tumors revealed a 10 times lower expression in the peptide treated tumor compared to the control tumor. However, in the tumors treated with both the peptide and 3-MA, Ki-67 expression was only reduced by a factor of 1.26 compared to the control tumor (Fig. 6 Ei and Eii).

Autophagy driven cell death by HAP and the peptides

Autophagy is widely acknowledged as a pro-survival mechanism within cells. however, emerging evidences indicate that it can also lead to cell death, a phenomenon referred to as type II programmed cell death. Considering the pivotal role of autophagy in metastasis and cancer cell survival, it is imperative to assess the impact of HAP and the peptides driven autophagy on the proliferation and survival of breast cancer cells.

Cell proliferation was quantified by measuring the expression of the proliferation marker Ki-67. Immunostaining of MCF7 and 4T1 cell lines demonstrated an alleviated expression of Ki-67 upon treatment with HAP and the peptides. Furthermore, when autophagy was inhibited using the autophagy inhibitor 3-MA, the previously determined effective dosages of HAP and the peptides failed to significantly abate Ki-67 expression (Fig. S3 Ai and Aii).

To investigate the impact of protease and peptide driven autophagy on cell viability, we conducted a 3-(4,5-dimethylthiazol-2-yl)-2,5-diphenyltetrazolium bromide (MTT) assay. We observed a reduction in survival of approximately 60% and 50% in MCF7 cells treated with HAP and the peptide PFAISED, respectively (Fig. S3 Bi). While, In the 4T1 cells, survival decreased by approximately 46% and 55% with HAP and the peptide PFISED, respectively

(Fig. S3 Bii). Consistent with our earlier findings in cell proliferation assay, the survivability also restored remarkably in both the cells when autophagy has been inhibited by 3-MA prior to the treatment with HAP and the peptides.

Discussion

Autophagy, long regarded as a fundamental cellular self-survival mechanism, has recently garnered more attention for its role in facilitating cell death as well, termed as type II programmed cell death [44-46]. This newfound understanding has led to the exploration of autophagy as a therapeutic target for a variety of diseases, including cancer and neurodegenerative conditions, where the selective elimination of specific cell populations is desired. Autophagy can be induced by a range of stimuli, indicating the presence of multiple upstream signaling pathways that may independently or in an intertwined manner govern autophagy [2]. In this study, we investigate the potential of a secreted metalloprotease, HAP, to induce targeted autophagy in mammalian breast cancer cells, alongside the signaling mechanisms involved.

HAP, owing to its proteolytic activity, engages with PARs on the membranes of various mammalian cancer cells. Previous studies from our group have demonstrated that HAP mediates the alternative activation of PAR1, a key mechanism driving HAP-induced apoptosis. Among the four known subtypes of PARs (PAR1, PAR2, PAR3, and PAR4), HAP specifically binds to PAR1 and activates it [32]. In the present study, we found that HAP induced autophagy in mammalian breast cancer cells at lower concentrations than those previously optimized for apoptosis induction, as reported by Ray *et al*. [31]. It is well-documented that a single stimulus can simultaneously regulate apoptotic and autophagic

pathways, with these processes often acting as mutually exclusive events [34, 35]. Upon further molecular analysis, we identified that the non-canonical activation of PAR1 by HAP is pivotal for the induction of autophagy. Interestingly, when apoptosis and autophagy are triggered by a common stimulus, autophagy is typically initiated as an early response, with apoptosis being recruited at later time points. In some instances, autophagy may even lead to apoptosis [34, 47].

PAR1 is a transmembrane G-protein-coupled receptor that, upon activation, interacts with a variety of G-protein subtypes, including G12/13, Gi, and Gq depending on the cellular context and modulates different signaling pathways [48-52]. Although PAR1 expression is minimal in most non-cancerous mammalian cells (with the exception of platelets), it is abundantly expressed in breast cancer cells, making it an ideal target for therapeutic intervention [53]. Thrombin, a serine protease, is a known activator of PAR1. It interacts with the receptor through its N-terminal exodomain, which contains two thrombin-binding sites [54]. Thrombin activates PAR1 by cleaving the Arg 41/Ser 42 site of its exodomain [39, 55]. G-protein coupled receptors are known to activate MAP kinases by signaling through G proteins and facilitate proliferation by mTOR activation [56]. This canonical pathway of PAR1 activation by thrombin also escalates proliferation via MAPK activation and leads to mTOR activation [27, 57]**,** which is considered as a negative regulator of autophagy [58]. Indeed, our findings suggested that activation of mTOR was consistent with the thrombin induced canonical activation of PAR1. However, we observed that HAP-treated cells exhibited a downregulation of mTOR activation, in contrast to thrombin's effects. Moreover, we found that thrombin failed to induce significant autophagic responses, whereas HAP demonstrated a marked ability to induce autophagy. We are reporting for the first time that non-canonical PAR1 activation by HAP induced autophagy, as opposed to its canonical

thrombin-mediated activation, which primarily upregulates mTOR activation that leads to cell proliferation.

Thrombin activates the human PAR1 homolog by proteolytically cleaving its N-terminal extracellular domain, which exposes a tethered ligand sequence (SFLLRN) that intramolecularly binds PAR1, initiating downstream signaling in platelets and vascular endothelial cells [55]. The murine homolog of PAR1 contains a similar sequence (SFFLRN) with the alteration of one amino acid (Phe 44 instead of Leu 44) at the same position. Earlier, our group have demonstrated that HAP cleaves the murine homolog of PAR1 at the Pro 90/Pro 91 site, resulting in the generation of a new N-terminal end with the sequence PFISED [32]. This sequence is analogous to PAFISED in the human PAR1 homolog, located between Leu 84 and Ala 92. Both PFISED and PAFISED peptides, designed on the basis of last seven and six amino acids of the N-terminal cleaved ends of human and murine homologs of PAR1 respectively, possess high affinity for their respective PAR1 homologs, as shown by molecular docking studies. The docking result and free energy findings suggest that these peptides were stable and potential candidates for cancer treatment.

Immunoblotting revealed that these peptides efficiently induced autophagy in breast cancer cells in a dose-dependent manner, while, the peptides SFLLRN and SFFLRN failed to induce autophagy.

Further investigation into the signaling pathways involved in autophagy induction by the PAFISED peptide in MCF7 cells revealed a significant downregulation of mTOR activation, as evidenced by a decrease in phosphorylated mTOR (p-mTOR), which resulted into a substantial decrease in p-ULK1^{Ser757} expression.

Collectively, the major three MAP kinases ERK1/2, p38 and JNK play a significant role in modulating mTOR activation. Given that mTOR is recognized as the master regulator of

autophagy, we deemed it essential to investigate the effects of the peptide PFAISED on these three MAP kinases activation. Immunoblot analyses confirmed significant downregulation of the phosphorylation of all the three MAP kinases, which justified the reduced expression of p-mTOR. However, peptide PAFISED upregulated the phosphorylation of AMPK, that led to an increase in the expression of p-ULK1^{Ser317} which facilitated the formation of initiation complex. An increased BECN1 expression upon the peptide treatment suggested the formation of nucleation complex. As the autophagy-inducing potential of the synthetic peptide that resembled the cleaved N-terminal end of non-canonically activated PAR1 was established, it became clear that the induction of autophagy was not HAP-specific, rather it depends on the site of cleavage on PAR1 exodomain.

A major limitation of many autophagy-inducing agents is their inability to form ALs or effectively degrade cargo. Our study confirmed that treatment with both HAP and peptides resulted in the formation of ALs in breast cancer cells. Degradation of cargoes is marked by the rupture of autolysosomal structure, which was evidenced by the elevated expression of Cathepsin L in cytosol. A downregulation of SQSTM1/p62 expression also confirmed the autophagosomal degradation of cargoes.

In the context of cancer therapy, it is crucial to ensure that autophagy induction leads to the cessation of cellular proliferation and a subsequent reduction in cancer cell survival. Our data showed a significant decline in both the proliferation rate and survival of breast cancer cells upon autophagy induction by HAP and the peptides. Notably, breast cancer cells, which exhibit high expression of PAR1, were selectively targeted by HAP and the peptide for induction of autophagy, while non-cancerous human breast epithelial cells remained unaffected.

We also assessed the *in vivo* impact of peptide-induced autophagy in low-grade breast cancer. Using the Nottingham Grading System, we classified tumors based on the scores given to them considering three aspects of the tumor tissue, *viz*. ductal/tubular/glandular differentiation, nuclear pleomorphism, and mitotic figure and correlated with the expression level of Ki-67. A cumulative score between 3-5 refers to a low-grade/grade I (well differentiated), while a cumulative score between 6-7 indicates an intermediate-grade/ grade II (moderately differentiated) breast cancer. A cumulative score between 8-9 signifies a high-grade/ grade III (poorly differentiated) breast cancer [43]. Our findings revealed that breast tumors developed in BALB/c mice with 4T1 cells remained well-differentiated (Grade I) up to 3 weeks. Following treatment with the PFISED peptide, we observed a significant hinderance of tumor growth and progression along with a partial cessation of increasing proliferation rate in this early-stage, low-grade breast cancer model. However, further studies on the physicochemical properties and *in vivo* toxicity assessments of the peptide are warranted before advancing to extensive and further clinical trials.

In conclusion, our study reveals that the non-canonical activation of PAR1 promotes autophagy in mammalian breast cancer cells through the inhibition of mTOR activation, in stark contrast to its canonical activation induced by thrombin, which stimulates cell proliferation by enhancing mTOR activation. Furthermore, we identified that a peptide resembling the newly formed N-terminal end of non-canonically activated PAR1 also triggers autophagy in these cells. This discovery opens new avenues for therapeutic strategies aimed at leveraging autophagy as a treatment modality for breast cancer, especially in its early stage.

Materials and methods

Bacterial strain growth conditions

The *Vibrio cholerae* O1 strain C6709 was selected for this study due to its harboring of a functional hapR gene, which encodes a regulatory protein that modulates several cellular processes in *Vibrio cholerae*, including the expression of hemagglutinin HAP [59]. Routine cultivation of *Vibrio cholerae* (C6709) was carried out in Luria broth (Himedia, M575) at 37□ with shaking for 18 h [60]. To preserve bacterial stocks, cells were stored at -70□ in Luria broth supplemented with 20% sterile glycerol (Sigma-Aldrich, G5516) [59].

Purification of the protease

HAP was isolated from *Vibrio cholerae* O1 strain C6709 and purified according to the protocol outlined by Ghosh *et al*. (2016) [61]. The *V. cholerae* O1 strain C6709 was grown and harvested as previously described. The cell-free culture supernatant was sequentially filtered through 0.45-µm and 0.22-µm cellulose acetate membranes (Merck, Darmstadt,

Germany, Product No. HAWP04700 and Product No. GSWP04700) to eliminate residual cells. Outer membrane vesicles were subsequently removed from the filtrate by ultracentrifugation at 150,000 x g for 3 h at 4□ using a T-865 rotor (Sorval Instruments, USA) [62]. The supernatant was carefully aspirated and subjected to salting out with 60% saturated ammonium sulfate (Sigma-Aldrich, St. Louis, Missouri, USA, Product No. A4418). Protein precipitation was achieved by centrifugation at 10,000 rotation per minute (RPM) for 20 mins at 4□. The resulting pellet was resuspended in 25 mM Tris (hydroxymethyl) aminomethane hydrochloride buffer (pH 7.4) (Sigma-Aldrich, St. Louis, Missouri, USA, Product No. 648317), dialyzed against the same buffer, and concentrated using an Amicon® Ultra Centrifugal Filter (Millipore, UFC9050). The protein was then purified through a single-step ion-exchange chromatography column (2.5 X 20 cm) packed with Diethylaminoethyl cellulose-52 (DEAE-52) matrix (Whatman, 4057050) and pre-equilibrated with 25 mM Tris (hydroxymethyl) aminomethane hydrochloride buffer (pH 7.4). Proteins were eluted in the unbound fractions, which formed distinct peaks, pooled, dialyzed, concentrated, and assayed for protease activity. Notably, the purification of HAP was performed without the use of Ethylenediamine tetraacetic acid (EDTA). Chromatographic separation was conducted using a Biologic Duo Flow Chromatographic System (Bio-Rad, USA). The purified HAP was stored in aliquots at -20□.

Sodium Dodecyl Sulfate-Polyacrylamide Gel Electrophoresis (SDS-PAGE)

SDS-PAGE was performed using the method described by Laemmli [63]. Protein samples were denatured in sample buffer and separated on a 12.5% polyacrylamide gel using a discontinuous buffer system.

Protease activity assay

In this study, azocasein (Sigma-Aldrich, A2765) was employed as a substrate to assess the proteolytic activity of HAP [64]. The substrate-enzyme mixture (azocasein-HAP) was incubated at 37□ for 1 hour, followed by termination of the reaction by the addition of 10% (w/v) trichloroacetic acid (Sigma-Aldrich, T8657). The precipitated protein was eliminated by centrifugation at 12,000 RPM for 4 mins, and the supernatant was transferred to a clean tube containing 525 mM sodium hydroxide. Absorbance was measured at 440 nm using a Shimadzu spectrophotometer (Shimadzu, Japan). Negative controls included the substrate with buffer and the substrate with EDTA-inactivated enzyme.

Cell culture

Human epithelial breast cancer cells MCF7 (ATCC, HTB-22), murine epithelial breast cancer cells 4T1 (ATCC, CRL-2539), and human normal breast epithelial cells MCF10A (ATCC, CRL-10317) were cultured (passages 10-12) and maintained in Minimum Essential Medium (MEM) (Gibco, 61100061), RPMI 1640 (Gibco, 23400021) and Mammary Epithelial Cell Basal Medium (MEBM) (Lonza, CC-3151) Mammary Epithelial Cell Growth Medium (MEGM) SingleQuots supplements (Lonza, CC-4136) respectively. Each medium was supplemented with 10% Fetal bovine serum (FBS) (Gibco, 10270106), 100 U/ml penicillin G, and 100 µg/ml streptomycin sulfate (Gibco, 15140122) and cells were incubated at 37□ in a 5% CO2 atmosphere using a Heracell incubator (Thermo Fisher Scientific, Waltham, MA, Catalog Number 51026331). The MCF7 and MCF10A cell lines were generously provided by Dr. Somsubhra Nath, Presidency University, Kolkata, while the 4T1 cell line was a gift from Dr. Saptak Banerjee, CNCI, Kolkata.

Western blotting

Western blotting was conducted as previously described by Nag *et al*. [65]. In brief, cultured cells were lysed using Radioimmunoprecipitation assay (RIPA) buffer (Sigma-Aldrich,

R0278), and protein concentrations were determined using the Bicinchonic acid (BCA) assay kit (Thermo Fisher Scientific, 23225). Equal amounts of protein were loaded onto SDS-PAGE for separation and subsequently transferred electrophoretically to a Polyvinylidene fluoride (PVDF) membrane (Merck, IPVH00010). Following transfer, the membrane was blocked with 3% Bovine serum albumin (BSA) (Sigma-Aldrich, A1470) in Tris-buffered saline (TBS) and incubated overnight at 4□ with the primary antibody (diluted according to the manufacturer's instructions) against the target protein. The blot was then washed with Tris-buffered saline-Tween 20 (TBST) buffer and incubated with Horseradish peroxidase (HRP)-conjugated secondary antibody (Cell Signaling Technology, 7076; 1:1000 and Cell Signaling Technology, 7074; 1:1000) for 2 h at room temperature. Protein bands were visualized using a Bio-Rad gel documentation system with an Enhanced chemiluminescence (ECL) substrate (Thermo Fisher Scientific, 34580) specific for HRP-conjugated antibodies. Western blot quantification was performed using GelQuant (Thermo Fisher Scientific, USA) and ImageJ (NIH, Bethesda, MD) software. At least three independent experiments were conducted to validate the results, and band intensities were normalized to loading controls: GAPDH for MCF7 and MCF10A cells, and Cyclophilin B for 4T1 cells.

Analyses of lysosomal and autophagosomal vacuoles by confocal microscopy

Lysosomal and autophagosomal vacuoles were analyzed by staining with LysoTracker™ Green DND-26 (Thermo Fisher Scientific, L7526), following the method described by Klepka *et al.* [66] with minor modifications tailored to the cell lines. Briefly, MCF7 and 4T1 cells were seeded onto cover slips in 6-well plates at a density of 0.3×10^5 cells per well. After 24 h of incubation, cells were treated with HAP (0.5 μg/ml for MCF7 and 0.75 μg/ml for 4T1) for 30 mins, with or without pre-treatment with 25 mM 3-MA, an autophagy inhibitor (Sigma-Aldrich, M9281) for 24 h. Untreated cells and those treated only with 3-MA served as normal and negative controls, respectively. Following HAP treatment, cells were

fixed with 4% paraformaldehyde for 10 mins at room temperature. They were then permeabilized with 0.1% Triton X-100 (Sigma-Aldrich, T8787) in 0.1% sodium citrate solution and blocked with 5% FBS prepared in TBST. The cells were incubated with LysoTracker™ Green DND-26 for 45 mins at 37□. Nuclei were stained with Hoechst 33342(Cell Signaling Technology, 4082; working concentration 1.0 μg/ml) for 10 mins at 37□. After washing twice, cells were mounted with 10% glycerol (Sigma-Aldrich, G5516). Images were acquired using a confocal microscope (Zeiss, Germany, LSM 710) with a Plan-Apochromat 63X / 1.40 NA objective. Data were processed and analyzed using Zen 3.4 (blue edition) and ImageJ software.

Autophagy detection by confocal microscopy and flow cytometry

Autophagy was detected by confocal microscopy using the Autophagy Assay Kit (Abcam, ab139484) according to the manufacturer's instructions. The kit contains a green fluorescent dye that specifically stains autophagosomal and autolysosomal vacuoles. Briefly, MCF7 and 4T1 cells were seeded onto cover slips in 6-well plates at a density of 0.3 × 10^5 cells per well. After 24 h of incubation, cells were treated with HAP (0.5 μg/ml for MCF7 and 0.75 μg/ml for 4T1) for 30 mins and with peptides (50μM dosage of PAFISED for MCF7 and 75 μM dosage of PFISED for 4T1) for 4 h. Following treatment, cells were washed twice with 1X Assay Buffer (diluted from the 10X stock provided with the kit) supplemented with 5% FBS. Cells were then incubated at 37□ for 30 mins with 100 μl of staining solution, which contained 2 μl of the green fluorescent dye and 1 μl of nuclear stain (Hoechst), both provided in the kit, in 1 ml of 1X Assay Buffer, supplemented with 5% FBS. After incubation, the staining solution was removed, and cells were washed twice with 1X Assay Buffer containing 5% FBS. Cells were then fixed with 4% formaldehyde for 15 mins and washed thrice with 1X Assay Buffer containing 5% FBS. Finally, cells were mounted on glass slides with 10% glycerol. Green fluorescence was detected using the FITC filter, and nuclear staining was

visualized using the DAPI filter on a confocal microscope (Zeiss, Germany, LSM 710) with a Plan-Apochromat 63X / 1.40 NA objective. Data were processed and analyzed using Zen 3.4 (blue edition) and ImageJ software.

The induction of autophagy was further analyzed by flow cytometry using the same Autophagy Assay Kit following the manufacturer's protocol. In a brief, cells were treated with HAP and the peptides as mentioned earlier and harvested by brief incubation with 0.25% trypsin-EDTA (Gibco, 25200072) at 37□. Cells were washed with 1X Assay Buffer, supplemented with 5% FBS, as outlined earlier and stained with 250 µl of the staining solution, comprising of 1 µl of the green fluorescent dye (provided in the kit) in 1 ml of 1X Assay Buffer supplemented with 5% FBS. Flowcytometry data were acquired using BD FACSAria™ II (BD, USA). Analyses of the flow cytometry data was performed using FloJo™ 10 software.

Immunocytochemistry and confocal imaging

Immunocytochemistry and confocal imaging were conducted following the procedures outlined by Nag *et al*. [65]. In brief, MCF7 and 4T1 cells were grown on coverslips in 6 well cell culture plates and treated with HAP (0.5 µg/ml for MCF7 and 0.75 µg/ml for 4T1) for 30 mins. Following the treatment, cells were fixed with 4% paraformaldehyde for 10 mins at room temperature. Cells were subsequently permeabilized using 0.1% Triton X-100 in 0.1% sodium citrate solution and blocked with TBST supplemented with 5% FBS for 2 h. They were incubated overnight at 4□ in a moist chamber with primary antibody (diluted according to the manufacturer's instructions) against the protein of interest. Following primary antibody incubation, cells were washed with TBS and incubated for 2 h at room temperature with Alexa 488 conjugated (Cell Signaling Technology, 4408; 1:200 and Cell Signaling Technology, 4412; 1:200) or Alexa 555 conjugated (Cell Signaling Technology, 4413; 1:200

and Cell Signaling Technology, 4409; 1:200) secondary antibodies. Nuclei were stained with Hoechst 33342 (Cell Signaling Technology, 4082; working concentration 1.0 µg/ml) for 10 mins at 37□. After washing the cells twice with TBS, they were mounted with 10% glycerol. Confocal images were captured using a confocal microscope (Zeiss, Germany, LSM 710) with a Plan-Apochromat 63X / 1.40 NA objective. Image processing and analyses were performed using Zen 3.4 (blue edition) and ImageJ software.

Raising of antisera against purified HAP

Antiserum against HAP was generated by immunizing a New Zealand White rabbit, following the method described by Mondal *et al*. [67]. The rabbit was initially administered an intramuscular injection of 100 mg of purified HAP emulsified with an equal volume of Freund's complete adjuvant (Sigma-Aldrich, F5881). This was followed by four booster injections of 100 mg of HAP emulsified with Freund's incomplete adjuvant (Sigma-Aldrich, St. Louis, Missouri, USA, Product No. F5506) at 7-day intervals. Blood samples were collected from the rabbit on day 0 and three days after the final booster injection, allowing the blood to clot overnight at room temperature. The sera were then collected, centrifuged (1,000 RPM for 5 mins), diluted in autoclaved glycerol, and stored at -80□ until use at a 1:1000 dilution.

Colocalization analyses by confocal imaging

Colocalization of HAP with PAR1 and of LAMP1 with LC3II was analyzed in HAP-treated (0.5 µg/ml for MCF7 and 0.75 µg/ml for 4T1 for 30 mins) and peptide-treated (50 µM of PAFISED for MCF7 and 75 µM of PFISED for 4T1 for 4 h) cells, respectively, by confocal microscopy, following the protocol described by Das *et al*. [68]. In brief, cells were grown on coverslips in 6 well cell culture plates. After the treatment, they were fixed with 4% paraformaldehyde for 10 mins at room temperature, and then permeabilized with 0.1% Triton

X-100 in 0.1% sodium citrate solution. The cells were blocked with 5% FBS in TBST for 2 h and incubated overnight at 4□ in a moist chamber with both of primary antibodies (diluted as per the manufacturer's instructions) against the respective proteins of interest. After washing twice with TBS, cells were incubated for 2 h at room temperature with Alexa 488 (Cell Signaling Technology, 4408; 1:200 and Cell Signaling Technology, 4412; 1:200) and Alexa 555 (Cell Signaling Technology, 4413; 1:200 and Cell Signaling Technology, 4409; 1:200) conjugated secondary antibodies. Nuclei were stained with Hoechst 33342 (Cell Signaling Technology, 4082; working concentration 1.0 μg/ml) for 10 mins at 37□. Following two washes with TBS, cells were mounted with 10% glycerol on a glass slide. Confocal images were acquired using a Zeiss LSM 710 microscope (Zeiss, Germany) with a Plan-Apochromat 63X / 1.40 NA objective. Image processing and analyses were performed using Zen 3.4 (blue edition) and ImageJ software. Colocalization was quantified by calculating Pearson's correlation coefficient.

Knock down of PAR1

MCF7 cells were first starved for 18 h in incomplete MEM before transfection. To transiently knock down PAR1, PAR1 siRNA (CGGUCUGUUAUGUGUCUAUdTdT) (Eurogentec, Seraing, Belgium) was used. Lipofectamine 3000 (Thermo Fisher Scientific, L3000001) served as the transfection reagent, and the procedure was carried out according to the manufacturer's instructions. Transfection was performed when the cells reached approximately 70% confluency. The transfection reagents were diluted in Opti-MEM (Gibco, 31985062) and added onto the cells dropwise. After 4 h, the medium was replaced with fresh complete MEM (supplemented with 10% FBS). PAR1 siRNA was transfected for 72 h to achieve efficient knockdown. Scrambled siRNA (Santa Cruz Biotechnology, sc-37007) was used as a control in this knockdown study. Knockdown efficiency was confirmed by Western blotting.

Flow cytometric analyses of lysosomal and autophagosomal vacuoles in PAR1 knocked down cells

Flow cytometry was employed to analyze lysosomal and autophagosomal vacuoles in HAP-treated WT and PAR1 KD MCF7 cells. Detection of these vacuoles was achieved by staining with LysoTracker™ Green DND-26 (Thermo Fisher Scientific, L7526), following the protocol outlined by Chikte *et al*. [69] with cell-specific optimization of dye concentration and incubation time. WT and PAR1 KD MCF7 cells were seeded at a density of 0.3×10^5 cells per well in 6-well tissue culture plates and were grown overnight. Both WT and PAR1 KD cells were treated with HAP at dosages of 0.5 μg/ml and 0.75 μg/ml for 30 as well as 60 mins. After treatment, cells were harvested by trypsinization (0.25% Trypsin-EDTA), washed twice with TBS, and resuspended in 500 μl of TBS. Cells were incubated with 60 nM LysoTracker™ Green DND-26 for 45 mins at 37□ for staining followed by washing with TBS twice. Finally, cells were resuspended in 500 μl of TBS and Flow cytometric analyses were conducted on the single cell populations, gated by forward scatter (FSC) and side scatter (SSC). The FITC channel (excitation at 488 nm and detection range of 515-545 nm) was used to identify LysoTracker™ Green DND-26-positive cells. Data acquisition was performed using a BD FACSAria™ II (BD, USA) and analyses were carried out using FloJo™ 10 software.

***in silico* analysis**

The crystal structure of human PAR1 bound to Vorapaxar (PDB ID: 3VW7) was retrieved from Protein Data Bank (https://www.rcsb.org) [70]. The physio-chemical properties, drug-likeness and pharmacokinetics of peptide were checked using swissADME (https://www.swissadme.ch) and toxicity was checked by ToxinPred (https://crdd.osdd.net/raghava/toxinpred**)** [71, 72]. After checking the peptides properties,

three servers were used one for peptide structure modelling and other two were used for molecular docking. Servers were PEP-FOLD4 (https://bioserv.rpbs.univ-paris-diderot.fr/services/PEP-FOLD4), Autodock Vina (https://www.swissdock.ch), CABS-dock (https://biocomp.chem.uw.edu.pl/CABSdock) [73-76]. PEP- FOLD4 was used for the peptide structure prediction; Autodock Vina and CABS-dock were used for the molecular docking in which Blind docking was performed by CABS-dock. The docking study was conducted in the following steps: - 1. Re-docked Vorapaxar by Autodock Vina [77], 2. Peptide docking against PAR 1 by Autodock Vina 3. Blind docking by CABS-dock 4. Binding interactions and analysis was performed by Biovia Discovery Studio visualizer 2024 (Dassault Systèmes BIOVIA, USA).

Transmission electron microscopy (TEM) imaging

For the TEM experiment, HAP and peptide treated and untreated MCF7 and 4T1 cells were washed three times in phosphate-buffered saline (PBS) and fixed with 2.5% glutaraldehyde in PBS (pH 7.4) overnight at 4□. The samples were then dyed with 2% uranyl acetate for 30□min, washed three times with distilled water and dehydrated for 15□min. Subsequently, the samples were embedded in EPON 812 resin (Head Biotechnology, E8000) and cured for 24□h at 70□. Ultrathin slices were procured using an ultramicrotome and then subjected to staining with a solution containing 2% uranyl acetate and lead citrate. The samples were imaged with a FEI Tecnai 12 BioTwin Transmission Electron Microscope operating at 100□kV.

Analysis of autophagy flux by pMXs GFP-LC3-RFP reporter construct

Autophagic flux in MCF7 and 4T1 cells treated with HAP and peptides was assessed by transiently expressing the pMXs GFP-LC3-RFP plasmid in these cells. This plasmid was originally cloned in NEB® Stable Competent E. coli (New England Biolabs, USA) and

obtained as an agarose stab culture as a generous gift from Noboru Mizushima Laboratory (Addgene, 117413) [41]. The plasmid was isolated using the QIAprep Spin Miniprep Kit (Qiagen, 27104) according to the manufacturer's protocol, and its purity was confirmed by agarose gel electrophoresis.

Prior to transfection, MCF7 and 4T1 cells were cultured on coverslips and subjected to starvation for 18 h in their respective media. Transfection was performed using Lipofectamine 3000 (Thermo Fisher Scientific, L3000001), following the manufacturer's protocol. Cells were transfected at approximately 70% confluency, and the all the reagents, including P3000, was added in Opti-MEM (Gibco, 31985062). After 4 h, the media was replaced with fresh complete media (supplemented with 10% FBS) suitable for the respective cell lines. MCF7 and 4T1 cells were transfected for 72 and 48 h, respectively, to ensure optimal transfection, which was confirmed by fluorescence microscopy. pAM_1C Empty Vector (Active Motiff, 53023) transfected cells were used as vehicle controls.

Following transfection, cells were treated with HAP (0.5 µg/ml for MCF7 and 0.75 µg/ml for 4T1) for 30 mins or with peptides (50 µM dosage of PAFISED for MCF7 and 75 µM dosage of PFISED for 4T1) for 4 h, and then fixed with 4% paraformaldehyde. After fixation, cells were stained with Hoechst 33342 (Cell Signaling Technology, 4082; working concentration 1.0 µg/ml) for 10 mins at 37□ and mounted with 10% glycerol on glass slides. Images were acquired using a confocal microscope (Zeiss, Germany, LSM 710) with a Plan-Apochromat 63X / 1.40 NA objective. Data processing was carried out using Zen 3.4 (blue edition) software, and the number of red and green puncta was quantified and analyzed using ImageJ software.

Cell viability and cell proliferation assay

MTT assay was conducted according to the standard protocol described by Kar *et al*. [78] to assess the effect of HAP and peptides (PAFISED for MCF7 and PFISED for 4T1 cells) on the cellular viability of breast cancer cells. Approximately 1×10^4 viable cells per well were seeded in flat bottom 96-well cell culture plates, where viability was determined using 0.4% Trypan blue solution (Thermo Fisher Scientific, 15250061) before seeding. After 24 h of incubation, MCF7 and 4T1 cells were treated with the optimized concentrations of HAP (0.5 μg/ml for MCF7 and 0.75 μg/ml for 4T1) for 30 mins and peptides (50 μM dosage of PAFISED for MCF7 and 75 μM dosage of PFISED for 4T1) for 4 h, with or without pre-treatment with 25 mM 3-MA, an autophagy inhibitor for 24 h. Following the treatment with HAP and the peptides, MTT solution (Thermo Fisher Scientific, M6494; 0.8 mg/ml in serum-free medium) was added, and cells were incubated for 4 h in the dark at 37□. The media was then removed, and 100 µl Dimethyl sulfoxide (Sigma-Aldrich, D5879) was added in each well to solubilize the purple crystal formazan. After a 15-minute incubation in the dark, absorbance was measured at 595 nm using a spectrophotomteric plate reader . The mean of three replicates was used to calculate the cell survival percentage.

To examine the impact of HAP- and peptide-induced autophagy on breast cancer cell proliferation, Ki-67 nuclear antigen immunofluorescence assay was performed in MCF7 and 4T1 cells following the standard protocol [79] with slight modifications optimized for the current experimental condition. Cells were treated with HAP and the respective peptides (PAFISED for MCF7 and PFISED for 4T1) as described above. After treatment, cells were fixed with 4% paraformaldehyde for 10 mins at room temperature, permeabilized with 0.1% Triton X-100 in 0.1% sodium citrate solution, and blocked with 5% serum in TBST. Cells were incubated overnight at 4□ with Ki-67 (D3B5) Rabbit mAb (Cell Signaling Technology, 9129; 1:400) in a moist chamber. Following washing with TBS, cells were incubated with Alexa 488-conjugated anti-rabbit IgG antibody (Cell Signaling Technology, 4412; 1:200).

Nuclei were stained with Hoechst 33342 (Cell Signaling Technology, 4082; working concentration 1.0 μg/ml) for 10 mins at 37□. After two additional washes with TBS, cells were mounted on glass slides with 10% glycerol. Images were captured using a confocal microscope (Zeiss, Germany, LSM 710) with a Plan-Apochromat 63X / 1.40 NA objective. Data were processed and analyzed using Zen 3.4 (blue edition) and ImageJ software.

***in vivo* experiments**

Animal model

In order to establish a low-grade breast tumor mouse model for studying the effect of the peptide (PFISED) induced autophagy in early stage breast cancer, first solid breast tumors were developed by implanting 4T1 cells in 7-8 weeks old female BALB/c mice following the protocol described by Pulaski *et al*. [80]. Briefly, Solid tumors were developed by implanting 4T1 cells ($0.5x10^4$ cells/ gram of body weight) subcutaneously at the abdominal mammary fat pad and allowed them to multiply. Cells were suspended in serum free RPMI 1640 media and each mouse was injected with 100 µl of the suspension. The mice were randomly distributed in six groups, each containing 5 mice (n=5). The groups were stratified based on the time which the tumors were harvested at after the implantation of 4T1 cells. (i) Group I: harvested the tumor at day 7, (ii) group II: harvested the tumor at day 14, (ii) group III: harvested the tumor at day 21, (iv) group IV: harvested the tumor at day 28, (v) group V: harvested the tumor at day 35, (vi) group VI: harvested the tumor at day 42. The day of tumour implantation was assigned as day ‘0’.

Tumors from all the groups were scored on the basis of histopathological analyses and grades were determined following the Nottingham Grading System [43, 81]. They have been further correlated immunohistochemically and with the size of the tumors.

Based on the gradation of malignancy, out of the three groups with low-grade tumor, group II (carrying tumor of 14 days) was selected randomly for further analyses to evaluate the role of the peptide (PFISED) induced autophagy in low-grade murine breast cancer. Three groups of experimental mice were designed, each group containing 5 mice, carrying breast tumor of 14 days. (i) Group I: without any treatment, considered as control, (ii) group II: injected with 5 mg/gram of body weight dosage of the peptide PFISED, (ii) group III: injected with the aforementioned dosage of peptide PFISED along with autophagy inhibitor, 3-MA (15 µg/gram of body weight). Mice of group II were injected with the peptide PFISED subcutaneously at the site of tumor at an interval of 3 days starting from the 14th day to 26th day after the implantation of 4T1 cells. In the mice of group III, 3-MA along with the peptide PFISED was administered according to the same experimental design of group II. The peptide PFISED and 3-MA were diluted in serum free RPMI 1640 and at one time each mouse was injected with 100 µl of the solution. Since, *in silico* analyses indicated that the peptide PFISED doesn't follow the Lipinski and Veber rules, the possibility of oral administration of the peptide had been excluded.

All the animal experiments and animal study design were approved by the institutional animal ethics committee (IAEC) of ICMR-National Institute of Research in Bacterial Infection (formerly ICMR-NICED) (License No: PRO/168/Jan 2022). Mice were procured from the animal breeding facility of ICMR-National Institute of Research in Bacterial Infection and were supplied with food pellets and autoclaved water ad libitum. When required, all the mice were euthanized via asphyxiation in a CO_2 chamber following the Committee for the Purpose of Control and Supervision of Experiments on Animals (CPCSEA) guidelines and the tumors were surgically excised.

Histology and immunohistochemistry

Immunohistochemical and hematoxylin-eosin (H&E) staining of tumor tissues was done as per protocol described by Kim *et al*. [82] with some minor modifications as required for the experiment. In a brief, tissues were fixed in 10% formaldehyde for at least 24 h and then processed by an automated tissue processor (Leica TP1020, Leica Microsystems, Germany). Processed tissues were embedded in paraffin and sectioned (5 µM thin) from the paraffin block by microtome, deparaffinized using xylene (Sigma-Aldrich, 6.08685), serially rehydrated and permeabilized with 0.5% Triton X-100 (Sigma-Aldrich, 93443) for 10 mins. Tissues were then incubated with 3% Hydrogen peroxide (H_2O_2) to inactivate the endogenous peroxidase activity and boiled in 10mM sodium citrate buffer pH 6.0 for 10 mins antigen retrieval. Tissue sections were blocked by incubating with TBST containing 5% FBS for 1 hour. They were stained with hematoxylin and eosin for histopathological analyses and for immunohistochemical analyses they were incubated with Ki-67 antibody (Cell Signaling Technology, 12202; 1:200) overnight in a humidified chamber at 4□, followed by an incubation with Alexa 488 conjugated goat anti-rabbit IgG antibody (Cell Signaling Technology, 4412) for 2 h at room temperature. Nuclei were stained with Hoechst.

Hematoxylin and eosin (H&E)-stained tissue sections were viewed under 20X magnification of Zeiss Axiovert 40 C microscope (Zeiss, Germany). Immunohistochemical images of randomly selected fields were captured using confocal microscope (Zeiss, Germany, LSM 710); objective-Plan-Apochromat 40X / 1.40 NA and quantified using Image J software.

Statistical analyses

All experiments were replicated at least three times ($n \geq 3$). All animal experimental groups contained 5 animals each. The experimental results were presented as mean ± standard error of mean (SEM). All statistical analyses were done by applying ordinary one-way ANOVA or two-way ANOVA or Student's t-test (Mann-Whitney test) or one sample t-test using

GraphPad Prism 10. In all the graph panels, ns (non-significant) $p \geq 0.05$, * (significant) $0.01 \leq p < 0.05$, ** (very significant) $0.001 \leq p < 0.01$, *** (extremely significant) $0.0001 \leq p < 0.001$, **** (extremely significant) $p < 0.0001$.

Generative AI

ChatGPT-4 has been employed to modify and improve the quality of language in some parts of the manuscript followed by rigorous manual revision.

List of key materials:

Reagent	Source	Identifier
Antibody		
LC3B antibody (for western blot)	Cell Signaling Technology	Cat. No. 2775
LC3B (E5Q2K) Mouse mAb (for immunofluorescence)	Cell Signaling Technology	Cat. No. 83506
LAMP1 (C54H11) Rabbit mAb (for western blot)	Cell Signaling Technology	Cat. No. 3243
LAMP1 (D2D11) XP® Rabbit mAb (for immunofluorescence)	Cell Signaling Technology	Cat. No. 9091
LAMP1 (E5N9Z) Rabbit mAb	Cell Signaling Technology	Cat. No. 99437
GAPDH (14C10) Rabbit mAb	Cell Signaling Technology	Cat. No. 2118
Cyclophilin B (D1V5J) Rabbit mAb	Cell Signaling Technology	Cat. No. 43603
Cathepsin L (E3R3P) Rabbit mAb	Cell Signaling Technology	Cat. No. 55914
Cathepsin L Polyclonal Antibody	Invitrogen	Cat. No. PA5-100424

Anti-PAR-1, clone ATAP2 Antibody	Merck Millipore	Cat. No. MABF244
SQSTM1/p62 Antibody	Cell Signaling Technology	Cat. No. 5114
Phospho-mTOR (Ser2448)	Cell Signaling Technology	Cat. No. 2971
mTOR Antibody	Cell Signaling Technology	Cat. No. 2972
Phospho-AMPK alpha-1,2 (Thr172) Polyclonal Antibody	Invitrogen	Cat. No. PA5-114550
AMPKα Antibody	Cell Signaling Technology	Cat. No. 2532
Reagent	**Source**	**Identifier**
Phospho-ULK1 (Ser757) Antibody	Cell Signaling Technology	Cat. No. 6888
Phospho-ULK1 (Ser317) Antibody	Cell Signaling Technology	Cat. No. 37762
ULK1 (D8H5) Rabbit mAb	Cell Signaling Technology	Cat. No. 8054
Beclin-1 Antibody	Cell Signaling Technology	Cat. No. 3738
p-ERK 1/2 Antibody (pT202/pY204.22A)	Santa Cruz Biotechnology	Cat. No. sc-136521
ERK 1/2 Antibody (C-9)	Santa Cruz Biotechnology	Cat. No. sc-514302
p-p38 MAPK Antibody (E-1)	Santa Cruz Biotechnology	Cat. No. sc-166182
p38 MAPK (D13E1) XP® Rabbit mAb	Cell Signaling Technology	Cat. No. 8690
p-JNK Antibody (G-7)	Santa Cruz Biotechnology	Cat. No. sc-6254
JNK Antibody (D-2)	Santa Cruz Biotechnology	Cat. No. sc-7345
Ki-67 (D3B5) Rabbit mAb	Cell Signaling Technology	Cat. No. 9129
Ki-67 (D3B5) Rabbit mAb (IHC Formulated)	Cell Signaling Technology	Cat. No. 12202
Anti-rabbit IgG, HRP-linked Antibody	Cell Signaling Technology	Cat. No. 7074
Anti-mouse IgG, HRP-linked Antibody	Cell Signaling Technology	Cat. No. 7076

Anti-mouse IgG (H+L), F(ab')$_2$ Fragment (Alexa Fluor® 488 Conjugate)	Cell Signaling Technology	Cat. No. 4408
Anti-rabbit IgG (H+L), F(ab')$_2$ Fragment (Alexa Fluor® 488 Conjugate)	Cell Signaling Technology	Cat. No. 4412
Anti-rabbit IgG (H+L), F(ab')$_2$ Fragment (Alexa Fluor® 555 Conjugate)	Cell Signaling Technology	Cat. No. 4413
Anti-mouse IgG (H+L), F(ab')$_2$ Fragment (Alexa Fluor® 555 Conjugate)	Cell Signaling Technology	Cat. No. 4409

Reagent	Source	Identifier
siRNA		
PAR1 siRNA (CGGUCUGUUAUGUGUCUAUdTdT)	Eurogentec	N/A
Scrambled siRNA	Santa Cruz Biotechnology	Cat. No. sc-37007
Peptide		
PAFISED	Eurogentec	N/A
PFISED	Eurogentec	N/A
SFLLRN	Eurogentec	N/A
SFFLRN	Eurogentec	N/A
Scrambled peptide (HTPPPPFISEDASGY)	Eurogentec	N/A
Plasmid		
pMXs GFP-LC3-RFP	Addgene	Cat. No. 117413
pAM_1C Empty Vector	Active Motiff	Cat. No. 53023

Acknowledgement

This research was generously supported by the Indian Council of Medical Research under the ad hoc project grant BMS/adhoc/56/2020-21, dated 23rd January 2021. Mr. Saibal Saha extends his sincere gratitude to the University Grants Commission, India, for awarding him the esteemed UGC-NET-JRF fellowship (UGC Ref. No.: 529/CSIR-UGC-NET JUNE 2019).

We are truly grateful to Dr. Santasabuj Das, Director of ICMR-NIRBI, for granting access to the central research instrumentation facility at ICMR-NIRBI. Our heartfelt thanks go to Dr. Somsubhra Nath (Presidency University, Kolkata, India) and Dr. Saptak Banerjee (CNCI, Kolkata, India) for their generous provision of cell lines. We are also thankful to Dr. Sushmita Bhattacharya (ICMR-NIRBI, India) for her invaluable inputs and suggestions in this study.

We would like to take the opportunity to express our gratitude to Dr. Sneha Mitra (ICMR-NIRBI, India) for her invaluable assistance in the analysis of flow cytometry data, and to Dr. Sarthak Das (A*STAR, Singapore) for his technical help in figure formatting. We also wish to acknowledge Mrs. Arpita Sarbajna (ICMR-NIRBI, India) and Ms. Anaswara Ramesh (ICMR-NIRBI, India) for their essential support during the transmission electron microscopy experiments.

Disclosure statements

Conflict of interest

The authors declare no conflict of interest.

Availability of data

The data presented in this study are available in the article and in the supplementary information. Any additional information required to reanalyse the data reported in this paper is available from the lead contact upon request. Information and requests for resources should be directed to and will be fulfilled by the lead contact, Dr. Amit Pal (pala.niced@gov.in/ palamit.app@gmail.com).

Author contributions

S.S. conceptualized and designed the study, performed experiments, analyzed and validated the data, wrote the original draft and reviewed. R.K. performed the *in silico* experiments and analyzed the data. S.S. analyzed the histopathological data. R.T. did formal analysis and reviewed the manuscript. T.R. assisted in performing experiments. A.G. provided technical assistance in confocal microscopy experiments. N.N. did formal analysis. A.P. helped in flow cytometric data acquisition and formal analysis. A.P. conceptualized the study, supervised the research work, helped in funding acquisition and data curation, reviewed and approved the final manuscript.

References

1. Yang, Z. and D.J. Klionsky, *Eaten alive: a history of macroautophagy.* Nat Cell Biol, 2010. **12**(9): p. 814-22.

2. Yin, Z., C. Pascual, and D.J. Klionsky, *Autophagy: machinery and regulation.* Microb Cell, 2016. **3**(12): p. 588-596.

3. Kelekar, A., *Autophagy.* Ann N Y Acad Sci, 2005. **1066**: p. 259-71.

4. Szeto, J., et al., *ALIS are stress-induced protein storage compartments for substrates of the proteasome and autophagy.* Autophagy, 2006. **2**(3): p. 189-99.

5. Iwata, J., et al., *Excess peroxisomes are degraded by autophagic machinery in mammals.* J Biol Chem, 2006. **281**(7): p. 4035-41.

6. Kim, P.K., et al., *Ubiquitin signals autophagic degradation of cytosolic proteins and peroxisomes.* Proc Natl Acad Sci U S A, 2008. **105**(52): p. 20567-74.

7. Novak, I., et al., *Nix is a selective autophagy receptor for mitochondrial clearance.* EMBO Rep, 2010. **11**(1): p. 45-51.

8. Ichimura, Y., et al., *Structural basis for sorting mechanism of p62 in selective autophagy.* J Biol Chem, 2008. **283**(33): p. 22847-57.

9. Pankiv, S., et al., *p62/SQSTM1 binds directly to Atg8/LC3 to facilitate degradation of ubiquitinated protein aggregates by autophagy.* J Biol Chem, 2007. **282**(33): p. 24131-45.

10. Kirkin, V., et al., *A role for NBR1 in autophagosomal degradation of ubiquitinated substrates*. Mol Cell, 2009. **33**(4): p. 505-16.

11. Parzych, K.R. and D.J. Klionsky, *An overview of autophagy: morphology, mechanism, and regulation.* Antioxid Redox Signal, 2014. **20**(3): p. 460-73.

12. Zhang, Q., et al., *Incomplete autophagy: Trouble is a friend.* Med Res Rev, 2022. **42**(4): p. 1545-1587.

13. Klionsky, D.J., et al., *Autophagy in major human diseases*. EMBO J, 2021. **40**(19): p. e108863.

14. Yun, C.W. and S.H. Lee, *The Roles of Autophagy in Cancer.* Int J Mol Sci, 2018. **19**(11).

15. Rosenfeldt, M.T. and K.M. Ryan, *The multiple roles of autophagy in cancer.* Carcinogenesis, 2011. **32**(7): p. 955-63.

16. Gewirtz, D.A., *The four faces of autophagy: implications for cancer therapy.* Cancer Res, 2014. **74**(3): p. 647-51.

17. Russell, R.C. and K.L. Guan, *The multifaceted role of autophagy in cancer.* EMBO J, 2022. **41**(13): p. e110031.

18. Deshmukh, R.R. and Q.P. Dou, *Proteasome inhibitors induce AMPK activation via CaMKKbeta in human breast cancer cells*. Breast Cancer Res Treat, 2015. **153**(1): p. 79-88.

19. Jiang, S., et al., *Participation of proteasome-ubiquitin protein degradation in autophagy and the activation of AMP-activated protein kinase.* Cell Signal, 2015. **27**(6): p. 1186-97.

20. Min, H., et al., *Bortezomib induces protective autophagy through AMP-activated protein kinase activation in cultured pancreatic and colorectal cancer cells.* Cancer Chemother Pharmacol, 2014. **74**(1): p. 167-76.

21. Kim, J., et al., *AMPK and mTOR regulate autophagy through direct phosphorylation of Ulk1*. Nat Cell Biol, 2011. **13**(2): p. 132-41.

22. Scherz-Shouval, R., et al., *The COOH terminus of GATE-16, an intra-Golgi transport modulator, is cleaved by the human cysteine protease HsApg4A.* J Biol Chem, 2003. **278**(16): p. 14053-8.

23. Tanida, I., et al., *GATE-16 and GABARAP are authentic modifiers mediated by Apg7 and Apg3*. Biochem Biophys Res Commun, 2003. **300**(3): p. 637-44.

24. Choy, A., et al., *The Legionella effector RavZ inhibits host autophagy through irreversible Atg8 deconjugation.* Science, 2012. **338**(6110): p. 1072-6.

25. Soh, U.J., et al., *Signal transduction by protease-activated receptors.* Br J Pharmacol, 2010. **160**(2): p. 191-203.

26. Flynn, A.N. and A.G. Buret, *Proteinase-activated receptor 1 (PAR-1) and cell apoptosis*. Apoptosis, 2004. **9**(6): p. 729-37.

27. Parrales, A., et al., *ERK1/2-dependent activation of mTOR/mTORC1/p70S6K regulates thrombin-induced RPE cell proliferation.* Cell Signal, 2013. **25**(4): p. 829-38.

28. Saxton, R.A. and D.M. Sabatini, *mTOR Signaling in Growth, Metabolism, and Disease.* Cell, 2017. **168**(6): p. 960-976.

29. Rabanal-Ruiz, Y., E.G. Otten, and V.I. Korolchuk, *mTORC1 as the main gateway to autophagy.* Essays Biochem, 2017. **61**(6): p. 565-584.

30. Elste, A.P. and I. Petersen, *Expression of proteinase-activated receptor 1-4 (PAR 1-4) in human cancer.* J Mol Histol, 2010. **41**(2-3): p. 89-99.

31. Ray, T., M.K. Chakrabarti, and A. Pal, *Hemagglutinin protease secreted by V. cholerae induced apoptosis in breast cancer cells by ROS mediated intrinsic pathway and regresses tumor growth in mice model.* Apoptosis, 2016. **21**(2): p. 143-54.

32. Ray, T. and A. Pal, *PAR-1 mediated apoptosis of breast cancer cells by V. cholerae hemagglutinin protease.* Apoptosis, 2016. **21**(5): p. 609-20.

33. Ray, T., et al., *Molecular targeting of breast and colon cancer cells by PAR1 mediated apoptosis through a novel pro-apoptotic peptide.* Apoptosis, 2018. **23**(11-12): p. 679-694.

34. Lockshin, R.A. and Z. Zakeri, *Apoptosis, autophagy, and more*. Int J Biochem Cell Biol, 2004. **36**(12): p. 2405-19.

35. Thorburn, A., *Apoptosis and autophagy: regulatory connections between two supposedly different processes.* Apoptosis, 2008. **13**(1): p. 1-9.

36. Crighton, D., et al., *DRAM, a p53-induced modulator of autophagy, is critical for apoptosis.* Cell, 2006. **126**(1): p. 121-34.

37. Arico, S., et al., *The tumor suppressor PTEN positively regulates macroautophagy by inhibiting the phosphatidylinositol 3-kinase/protein kinase B pathway.* J Biol Chem, 2001. **276**(38): p. 35243-6.

38. Kaminskyy, V. and B. Zhivotovsky, *Proteases in autophagy.* Biochim Biophys Acta, 2012. **1824**(1): p. 44-50.

39. Chen, J., et al., *Thrombin receptor activation. Confirmation of the intramolecular tethered liganding hypothesis and discovery of an alternative intermolecular liganding mode*. J Biol Chem, 1994. **269**(23): p. 16041-5.

40. Mizushima, N., *The role of the Atg1/ULK1 complex in autophagy regulation.* Curr Opin Cell Biol, 2010. **22**(2): p. 132-9.

41. Morita, K., et al., *Genome-wide CRISPR screen identifies TMEM41B as a gene required for autophagosome formation.* J Cell Biol, 2018. **217**(11): p. 3817-3828.

42. Lin, F., Y.T. Zhu, and Z.H. Qin, *Biomarkers of Autophagy.* Adv Exp Med Biol, 2021. **1208**: p. 265-287.

43. van Dooijeweert, C., P.J. van Diest, and I.O. Ellis, *Grading of invasive breast carcinoma: the way forward.* Virchows Arch, 2022. **480**(1): p. 33-43.

44. Liu, S., et al., *Autophagy: Regulator of cell death.* Cell Death Dis, 2023. **14**(10): p. 648.

45. Green, D.R., *The Coming Decade of Cell Death Research: Five Riddles.* Cell, 2019. **177**(5): p. 1094-1107.

46. Hou, W., et al., *Autophagy promotes ferroptosis by degradation of ferritin.* Autophagy, 2016. **12**(8): p. 1425-8.

47. Nikoletopoulou, V., et al., *Crosstalk between apoptosis, necrosis and autophagy.* Biochim Biophys Acta, 2013. **1833**(12): p. 3448-3459.

48. Vouret-Craviari, V., et al., *Regulation of the actin cytoskeleton by thrombin in human endothelial cells: role of Rho proteins in endothelial barrier function.* Molecular biology of the cell, 1998. **9**(9): p. 2639-2653.

49. Taylor, S.J., et al., *Activation of the β1 isozyme of phospholipase C by α subunits of the Gq class of G proteins.* Nature, 1991. **350**(6318): p. 516-518.

50. Offermanns, S., et al., *G proteins of the G12 family are activated via thromboxane A2 and thrombin receptors in human platelets.* Proceedings of the National Academy of Sciences, 1994. **91**(2): p. 504-508.

51. Klages, B., et al., *Activation of G12/G13 results in shape change and Rho/Rho-kinase–mediated myosin light chain phosphorylation in mouse platelets.* The Journal of cell biology, 1999. **144**(4): p. 745-754.

52. Hung, D., et al., *The cloned platelet thrombin receptor couples to at least two distinct effectors to stimulate phosphoinositide hydrolysis and inhibit adenylyl cyclase.* Journal of Biological Chemistry, 1992. **267**(29): p. 20831-20834.

53. Boire, A., et al., *PAR1 is a matrix metalloprotease-1 receptor that promotes invasion and tumorigenesis of breast cancer cells.* Cell, 2005. **120**(3): p. 303-13.

54. Nieman, M.T. and A.H. Schmaier, *Interaction of thrombin with PAR1 and PAR4 at the thrombin cleavage site.* Biochemistry, 2007. **46**(29): p. 8603-10.

55. Vu, T.K., et al., *Molecular cloning of a functional thrombin receptor reveals a novel proteolytic mechanism of receptor activation.* Cell, 1991. **64**(6): p. 1057-68.

56. Lopez-Ilasaca, M., *Signaling from G-protein-coupled receptors to mitogen-activated protein (MAP)-kinase cascades*. Biochem Pharmacol, 1998. **56**(3): p. 269-77.

57. Wang, H., et al., *Thrombin (PAR-1)-induced proliferation in astrocytes via MAPK involves multiple signaling pathways.* Am J Physiol Cell Physiol, 2002. **283**(5): p. C1351-64.

58. Jung, C.H., et al., *mTOR regulation of autophagy.* FEBS Lett, 2010. **584**(7): p. 1287-95.

59. Jobling, M.G. and R.K. Holmes, *Characterization of hapR, a positive regulator of the Vibrio cholerae HA/protease gene hap, and its identification as a functional homologue of the Vibrio harveyi luxR gene.* Mol Microbiol, 1997. **26**(5): p. 1023-34.

60. Saha, A., S. Haralalka, and R.K. Bhadra, *A naturally occurring point mutation in the 13-mer R repeat affects the oriC function of the large chromosome of Vibrio cholerae O1 classical biotype.* Arch Microbiol, 2004. **182**(5): p. 421-7.

61. Ghosh, A., H. Koley, and A. Pal, *The Role of Vibrio cholerae Haemagglutinin Protease (HAP) in Extra-Intestinal Infection.* J Clin Diagn Res, 2016. **10**(9): p. DC10-DC14.

62. Lin, C.-J., et al., *Non-O1 Vibrio cholerae bacteremia in patients with cirrhosis: 5-yr experience from a single medical center.* American Journal of Gastroenterology (Springer Nature), 1996. **91**(2).

63. Laemmli, U.K., *Cleavage of structural proteins during the assembly of the head of bacteriophage T4*. Nature, 1970. **227**(5259): p. 680-5.

64. Ghosh, A., et al., *Enterotoxigenicity of mature 45-kilodalton and processed 35-kilodalton forms of hemagglutinin protease purified from a cholera toxin gene-negative Vibrio cholerae non-O1, non-O139 strain*. Infect Immun, 2006. **74**(5): p. 2937-46.

65. Nag, N., et al., *Metallo-protease Peptidase M84 from Bacillusaltitudinis induces ROS-dependent apoptosis in ovarian cancer cells by targeting PAR-1*. iScience, 2024. **27**(6): p. 109828.

66. Klepka, C., et al., *Impairment of lysosomal function by Clostridioides difficile TcdB.* Mol Microbiol, 2022. **117**(2): p. 493-507.

67. Mondal, A., et al., *Cytotoxic and Inflammatory Responses Induced by Outer Membrane Vesicle-Associated Biologically Active Proteases from Vibrio cholerae.* Infect Immun, 2016. **84**(5): p. 1478-1490.

68. Das, R., et al., *MITOL-mediated DRP1 ubiquitylation and degradation promotes mitochondrial hyperfusion in a CMT2A-linked MFN2 mutant.* J Cell Sci, 2022. **135**(2).

69. Chikte, S., N. Panchal, and G. Warnes, *Use of LysoTracker dyes: a flow cytometric study of autophagy.* Cytometry Part A, 2014. **85**(2): p. 169-178.

70. Zhang, C., et al., *High-resolution crystal structure of human protease-activated receptor 1*. Nature, 2012. **492**(7429): p. 387-92.

71. Daina, A., O. Michielin, and V. Zoete, *SwissADME: a free web tool to evaluate pharmacokinetics, drug-likeness and medicinal chemistry friendliness of small molecules.* Sci Rep, 2017. **7**: p. 42717.

72. Gupta, S., et al., *In silico approach for predicting toxicity of peptides and proteins*. PLoS One, 2013. **8**(9): p. e73957.

73. Rey, J., et al., *PEP-FOLD4: a pH-dependent force field for peptide structure prediction in aqueous solution.* Nucleic Acids Res, 2023. **51**(W1): p. W432-W437.

74. Eberhardt, J., et al., *AutoDock Vina 1.2.0: New Docking Methods, Expanded Force Field, and Python Bindings.* J Chem Inf Model, 2021. **61**(8): p. 3891-3898.

75. Trott, O. and A.J. Olson, *AutoDock Vina: improving the speed and accuracy of docking with a new scoring function, efficient optimization, and multithreading.* J Comput Chem, 2010. **31**(2): p. 455-61.

76. Kurcinski, M., et al., *CABS-dock standalone: a toolbox for flexible protein-peptide docking.* Bioinformatics, 2019. **35**(20): p. 4170-4172.

77. Hidayat, A.N., et al., *Insight into human protease activated receptor-1 as anticancer target by molecular modelling.* SAR QSAR Environ Res, 2015. **26**(10): p. 795-807.

78. Kar, S., et al., *Expression profiling of DNA methylation-mediated epigenetic gene-silencing factors in breast cancer.* Clin Epigenetics, 2014. **6**(1): p. 20.

79. Li, S., et al., *ELAVL4 promotes the tumorigenesis of small cell lung cancer by stabilizing LncRNA LYPLAL1-DT and enhancing profilin 2 activation.* FASEB J, 2023. **37**(10): p. e23170.

80. Pulaski, B.A. and S. Ostrand□Rosenberg, *Mouse 4T1 breast tumor model.* Current protocols in immunology, 2000. **39**(1): p. 20.2. 1-20.2. 16.

81. Boiesen, P., et al., *Histologic grading in breast cancer--reproducibility between seven pathologic departments. South Sweden Breast Cancer Group.* Acta Oncol, 2000. **39**(1): p. 41-5.

82. Kim, A., et al., *The prognostic significance of tumor-infiltrating lymphocytes assessment with hematoxylin and eosin sections in resected primary lung adenocarcinoma.* PLoS One, 2019. **14**(11): p. e0224430.

Table 1: Analysis of the grade of tumors of different experimental groups

Tumor sample	Ductal/tubular/glandular differentiation	Nuclear pleomorphism	Mitotic figure	Cumulative score	Grade of tumor

Control	2	3	1	6	II
Tumor treated with peptide PFISED	2	2	1	5	II
Tumor treated with 3-MA and peptide PFISED	1	1	1	3	I

Scores of the experimental sets of tumors, assigned upon histopathological analysis of the three parameters, *viz*. Ductal/tubular/glandular differentiation, Nuclear pleomorphism and Mitotic figure and gradation of tumors based on their cumulative scores following Nottingham Grading System.

Figure legends

Figure 1: A dose-dependent induction of autophagy by HAP in mammalian breast cancer cells. **(Ai)** Representative immunoblots of markers of autophagy, *viz*. LAMP1 and LC3 in whole cell lysate of MCF-7 and 4T1 treated with different dosages of HAP (0.25, 0.5, 0.75

and 1 μg/ml) for two different time points (30 mins and 60 mins). **(Aii)** Quantification of the protein level of LAMP1 normalized against GAPDH (in MCF-7) and Cyclophilin B (in 4T1) and LC3 II:LC3 I ratio by densitometric analysis. **(Bi)** Representative confocal microscopy images of immunofluorescence of LysoTracker^{TM} in MCF-7 and 4T1 cells treated with the optimized dosage of HAP (0.5 μg/ml for 30 minutes in MCF-7 and and 0.75 μg/ml for 30 minutes in 4T1) along with or without the pretreatment of the autophagy inhibitor 3MA **(Bii)** Quantification of the mean fluorescence intensity of LysoTracker^{TM} per cell. **(Ci)** Representative fluorescent images of MCF-7 and 4T1 cells treated with the previously optimized dosages of HAP stained using Autophagy assay kit of Abcam (ab139484) and captured using the FITC channel of a confocal microscope. **(Cii)** Quantification of the mean fluorescence intensity of FITC per cell.

Figure 2: Involvement of PAR-1 in HAP induced autophagy. **(Ai)** Representative immunoblots of PAR-1 using whole cell lysate of MCF-7 and 4T1 treated with different dosages of HAP (0.25, 0.5, 0.75 and 1 μg/μl) for two different time points (30 mins and 60 mins). **(Aii)** Quantification of the protein level of PAR-1 normalized against GAPDH (in MCF-7) and Cyclophilin B (in 4T1). **(Bi)** Confocal microscopic immunofluorescent images of MCF-7 and 4T1 cells demonstrating colocalization of HAP and PAR-1.HAP was detected with antisera raised against HAP and PAR-1 was detected with anti-PAR1 antibody tagged with Alexa Fluor 488 and Alexa Fluor 647 respectively. **(Bii)** Quantification of colocalization of HAP and PAR-1 in term of Pearson's correlation coefficient and represented in graphical form. **(Ci)** Representative immunoblots of PAR-1 using whole cell lysate of wild type MCF-7 cells and siRNA mediated PAR-1 knocked down MCF-7 cells. **(Cii)** Quantification of the protein level of PAR-1 normalized against GAPDH by densitometry. **(Di)** Representative immunoblots of SQSTM1/p62 and LC3 using whole cell lysate of wild type and PAR-1

knocked down MCF-7 cells, both treated with two different dosages of HAP for two different time points (0.5 μg/ml for 30 minutes and 0.25 μg/ml for 60 minutes). **(Dii)** Quantification of protein level of SQSTM1/p62 normalized against GAPDH and LC3II:LC3I ratio by densitometry. **(Ei)** Representative flow cytometric images of wild type and PAR-1 knocked down MCF-7 cells, both treated with different dosages of HAP for two different time points (0.5 and 0.75 μg/ml for 30 minutes and 0.25 and 0.5 μg/ml for 60 mins) and stained with LysoTracker™. **(Eii)** Quantification of the percent positive cells for LysoTracker™ staining.

Figure 3: Docking analysis of peptide against the PAR1 receptor. **(A)** Crystal structure of PAR1 (3VW7) with Vorapaxar with their binding interaction. **(B)** Result of re-docked Vorapaxar with binding interaction and superimposed pose of re-docked Vorapaxar (in yellow) with binding parameters that used in Autodock Vina. Docking Score = -13.136 kcal/mol **(C)** 2-D structure of peptide **(Ci)** PAFISED and **(Cii)** PFISED and hydrogen bond donor interaction of docked peptide with SAS view and their binding interaction of PAFISED AND PFISED respectively.

Figure 4: Molecular signalling mechanism of the peptide induced autophagy. **(Ai)** Immunoblots of LC3, LAMP1, p-mTOR and mTOR in whole cell lysates of MCF-7 and 4T1 treated with HAP (0.5 and 0.75 μg/ml in MCF-7 and 4T1 respectively) for 30 mins and thrombin (10 nmol/L for 3 hours). **(Aii)** Densitometric analysis of the protein expression of LC3II:LC3I, p-mTOR/mTOR and LAMP1 normalized against GAPDH in MCF-7 and against Cyclophilin B in 4T1. **(Bi)** Immunoblots of SQSTM1/p62 in the whole cell lysates of MCF-7 and 4T1, where MCF7 cells treated with the synthetic peptides PFAISED (50 μM), SFLLRN (50 μM) and scramble peptide (HTPPPPFISEDASGY) and 4T1 cells with PFISED

(75 μM), SFFLRN (75 μM) and scramble peptide (HTPPPPFISEDASGY) for 4 hours. **(Bii)** Quantitative analysis of the expression of SQSTM1/p62 normalized against GAPDH (in MCF-7) and Cyclophilin B (in 4T1). **(Ci)** Representative images of the immunoblots of the autophagy markers LC3, LAMP1 and SQSTM1/p62 in whole cell lysates of MCF-7 and 4T1 treated with different dosages (5, 25, 50, 75 and 100 μM) of both the peptides PFAISED and PFISED for 4 hours. **(Cii)** Densitometric analysis of the expression of LC3II:LC3I and LAMP1 & SQSTM1/p62 normalized against GAPDH (in MCF-7) and Cyclophilin B (in 4T1). **(Di)** Representative immunofluorescence images of MCF-7 and 4T1 cells. MCF-7 cells were treated with the peptide PFAISED (50 μM) and 4T1 cells were treated with the peptide PFISED (75 μM) for 4 hours and stained using dyes included in the Autophagy assay kit (ab139484) of Abcam and observed in a confocal microscope under FITC channel. **(Dii)** Quantification of the Mean fluorescence intensity of green fluorescence (FITC) per cell. **(Ei)** Representative immunoblots of different signalling molecules of autophagy including p-mTOR, mTOR, p-AMPK, AMPK, p-ULK1 (Ser757), p-ULK1 (Ser317), ULK-1 and Beclin1 in the whole cell lysate of MCF-7 treated with different dosages of the peptide PFAISED, ranging from 5μM to 100 μM. **(Eii)** Quantification of p-mTOR/mTOR, p-AMPK/AMPK, p-ULK1 (Ser757)/ULK1, P-ULK1 (Ser317)/ULK1 and Beclin1 normalized against GAPDH by densitometric analysis. **(Fi)** Representative immunoblots of the three MAP kinase molecules Erk1/2, p38 and Jnk and their phosphorylated forms in the whole cell lysate of MCF-7 treated with different dosages of the peptide PFAISED, ranging from 5μM to 100 μM. **(Fii)** Quantitative analysis of the expression of p-Erk1/2/ Erk, p-p38/p38 and p-Jnk/Jnk by densitometry.

Figure 5: Formation of autolysosome and analysis of autophagy flux. **(Ai)** Representative confocal microscopic immunofluorescent images of MCF-7 and 4T1 cells transfected with

the plasmid construct pMXs GFP-LC3-RFP and treated with HAP (0.5 and 0.75 μg/ml for MCF-7 and 4T1 respectively) for 30 minutes and with the peptides (50 Mm of PAFISED for MCF-7 and 75 μM of PFISED for 4T1) for 4 hours. pAM_1C empty vector transfected cells were kept as control. **(Aii)** Ratio of the mean of numbers of red puncta (RFP) and green puncta (GFP in non-acidic enviroment) per cell was measured and graphically presented. **(Bi)** Immunofluorescent images of MCF-7 and 4T1 treated with peptides (PFAISED of 50 μM and PFISED of 75 μM for MCF-7 and 4T1 respectively) and stained against LAMP1 and LC3II with anti-LAMP1 and anti-LC3 antibodies and incubated them with their respective secondary antibodies tagged with AlexaFluor 555 and AlexaFluor 488 respectively. (Cii) Colocalization of AlexaFluor 555 tagged LAMP1 and AlexaFluor 488 tagged LC3II was measured in term of Pearson's correlation coefficient and graphically presented. **(C)** Representative transmission electron microscopic (TEM) images of MCF-7 and 4T1 treated with HAP (0.5 μg/ml for MCF-7 and 0.75 μg/ml for 4T1) for 30 minutes and with peptides (50 Mm of PAFISED for MCF-7 and 75 μM of PFISED for 4T1) for 4 hours. Autophagosomal structures (AP) and autolysosomal structures (AL) are marked with arrows.

Figure 6: *in vivo* analysis of the impact of peptide induced autophagy on low-grade breast tumor. **(A)** Graphical representation of the *in vivo* experimental design. **(B)** Comarative survivability percentage of four sets of BALB/c mice, *viz*. control: mice without tumor, tumor control: mice bearing 4T1 induced tumor but without any treatment, tumor+peptide: tumor-bearing mice treated with the peptide PFISED (5 mg/gram body weight) periodically at an interval of 3 days from day 14 to day 26 after the administration of 4T1 cells, tumor+3-MA+peptide: tumor-bearing mice treated with the peptide PFISED as described before with a simultaneous treatment of autophagy inhibitor 3-MA. **(Ci)** Images of the solid tumors from the aforementioned three groups of mice, *viz*. tumor control, tumor+peptide and tumor+3-

MA+peptide. **(Cii)** Comparative analysis of the volume of the tumors from these three groups of mice. **(D)** Histological images of tumors from these three groups of mice. Images were captured using inverted light microscope with 20X (first image of every row) and 40X magnification (second image of every row). Glandular/tubular differentiations are marked with purple arrow in the first image of every row and nuclear pleomorphisms are marked with green arrow in the second image of every row. **(Ei)** Immunofluorescence images of the expression of the proliferation marker Ki-67 in the tumors of aforementioned three groups of mice. Tumor samples were immunohistochemically analyzed with anti-Ki-67 antibody, further incubated with AlexaFluor 488 tagged secondary antibody and images were captured under FITC channel of a confocal microscope. Nuclei were stained with Hoechst 33342. **(Eii)** Graphical presentation of comparative analysis of the expression of Ki-67 in all three tumor sets.

Figure 7: Graphical abstract of signaling pathway of autophagy induced by HAP mediated non-canonical activation of PAR1

Figures

Figure 1

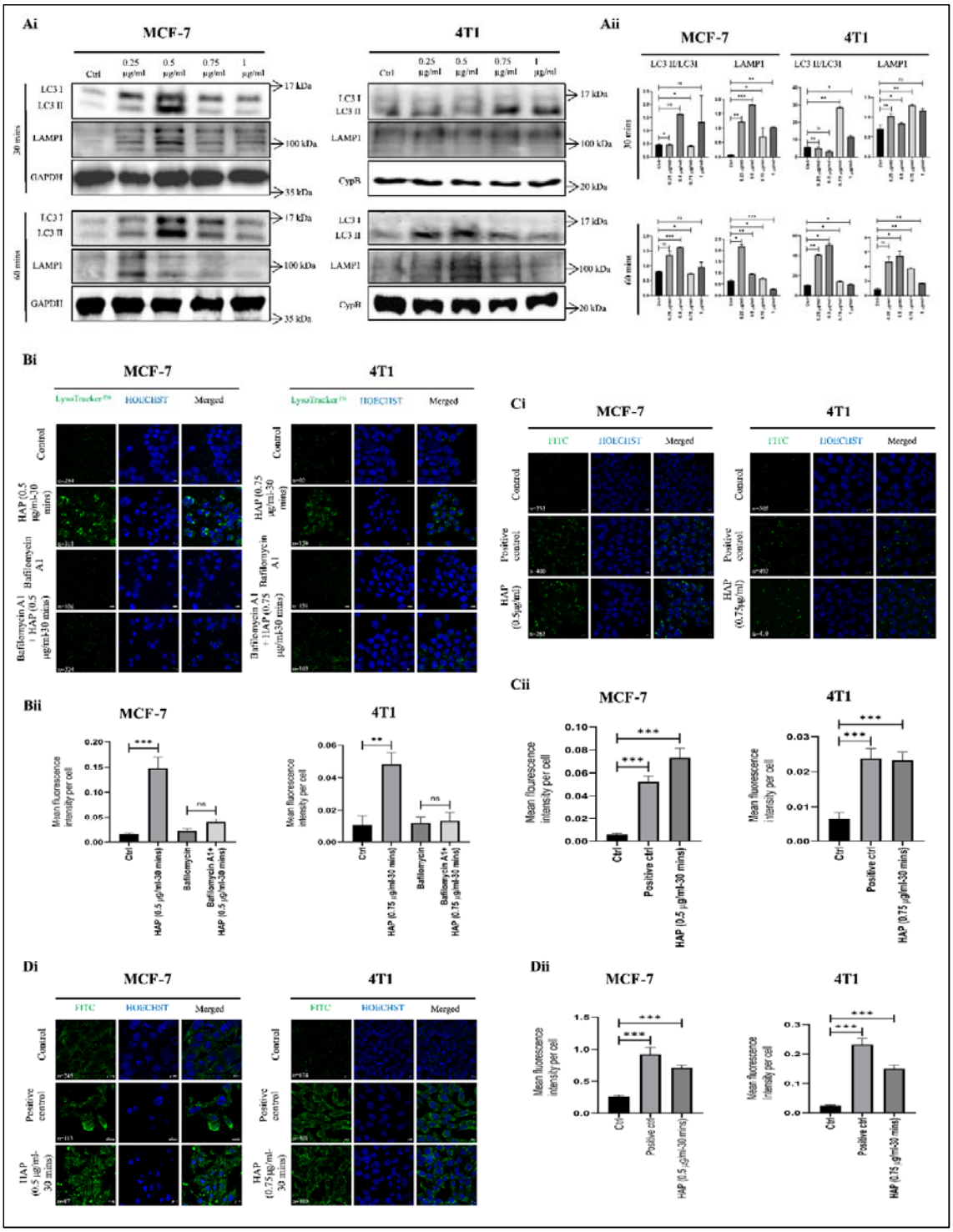

Figure 2

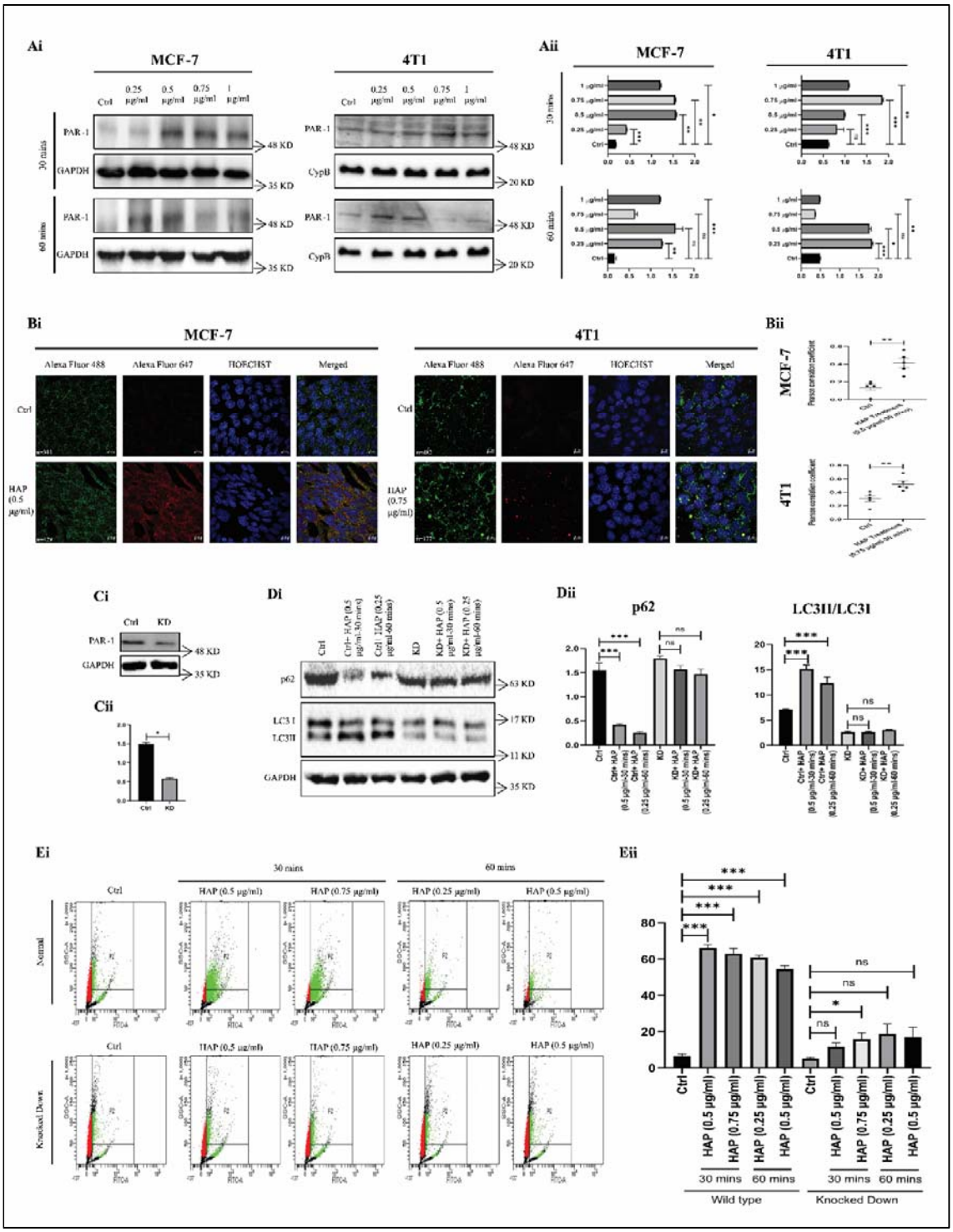
Ai
MCF-7
4T1
Ctrl
0.25 μg/ml
0.5 μg/ml
0.75 μg/ml
1 μg/ml
30 mins
60 mins
PAR-1
GAPDH
CypB
48 KD
35 KD
20 KD
Aii
Bi
Alexa Fluor 488
Alexa Fluor 647
HOECHST
Merged
HAP (0.5 μg/ml)
HAP (0.75 μg/ml)
Bii
Ci
KD
Cii
Di
p62
LC3I
LC3II
63 KD
17 KD
11 KD
Dii
LC3II/LC3I
Ei
Normal
Knocked Down
HAP (0.5 μg/ml)
HAP (0.75 μg/ml)
HAP (0.25 μg/ml)
Eii
Wild type
Knocked Down

Figure 3

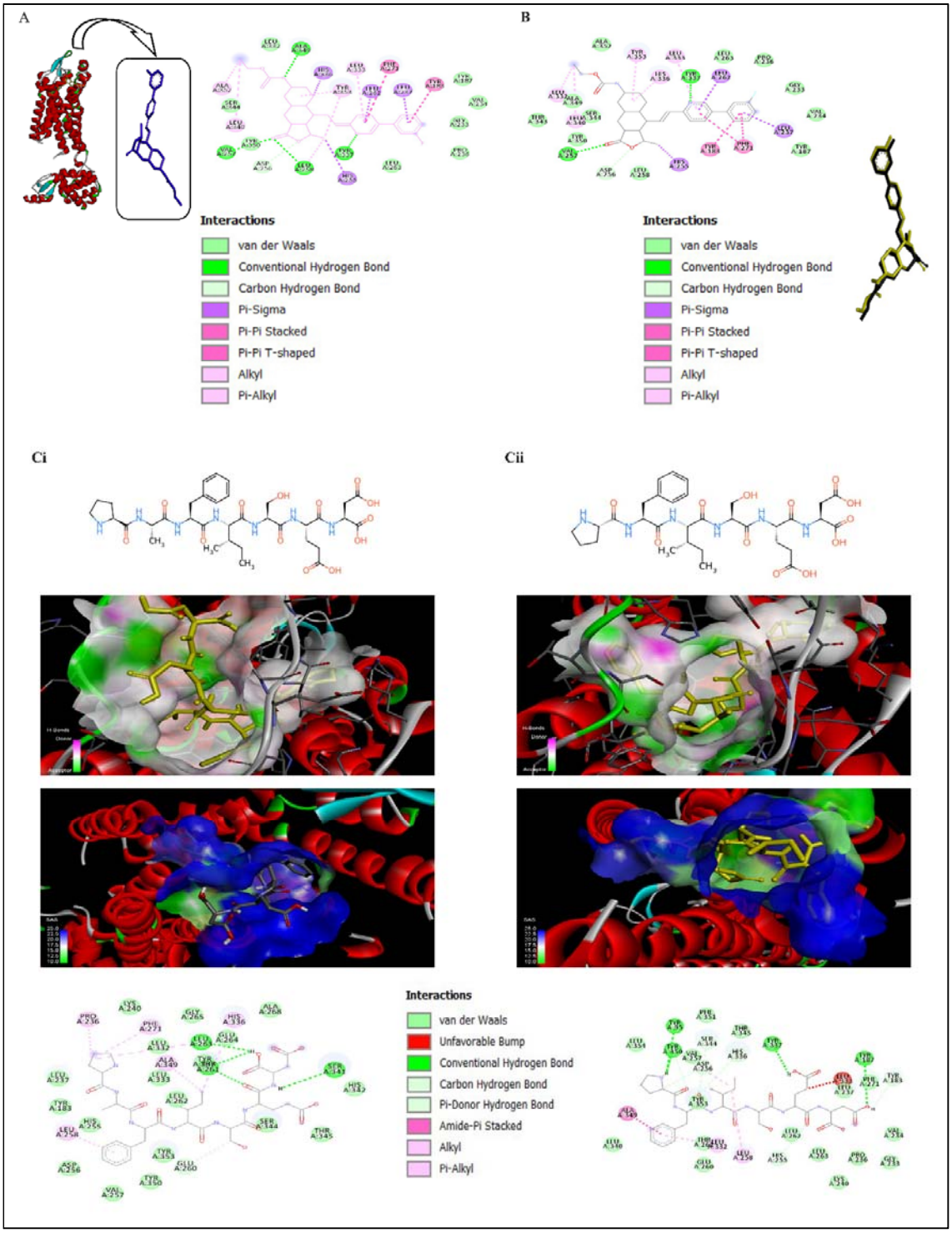
A
Interactions
van der Waals
Conventional Hydrogen Bond
Carbon Hydrogen Bond
Pi-Sigma
Pi-Pi Stacked
Pi-Pi T-shaped
Alkyl
Pi-Alkyl
B
Interactions
van der Waals
Conventional Hydrogen Bond
Carbon Hydrogen Bond
Pi-Sigma
Pi-Pi Stacked
Pi-Pi T-shaped
Alkyl
Pi-Alkyl
Ci
Cii
Interactions
van der Waals
Unfavorable Bump
Conventional Hydrogen Bond
Carbon Hydrogen Bond
Pi-Donor Hydrogen Bond
Amide-Pi Stacked
Alkyl
Pi-Alkyl

Figure 4

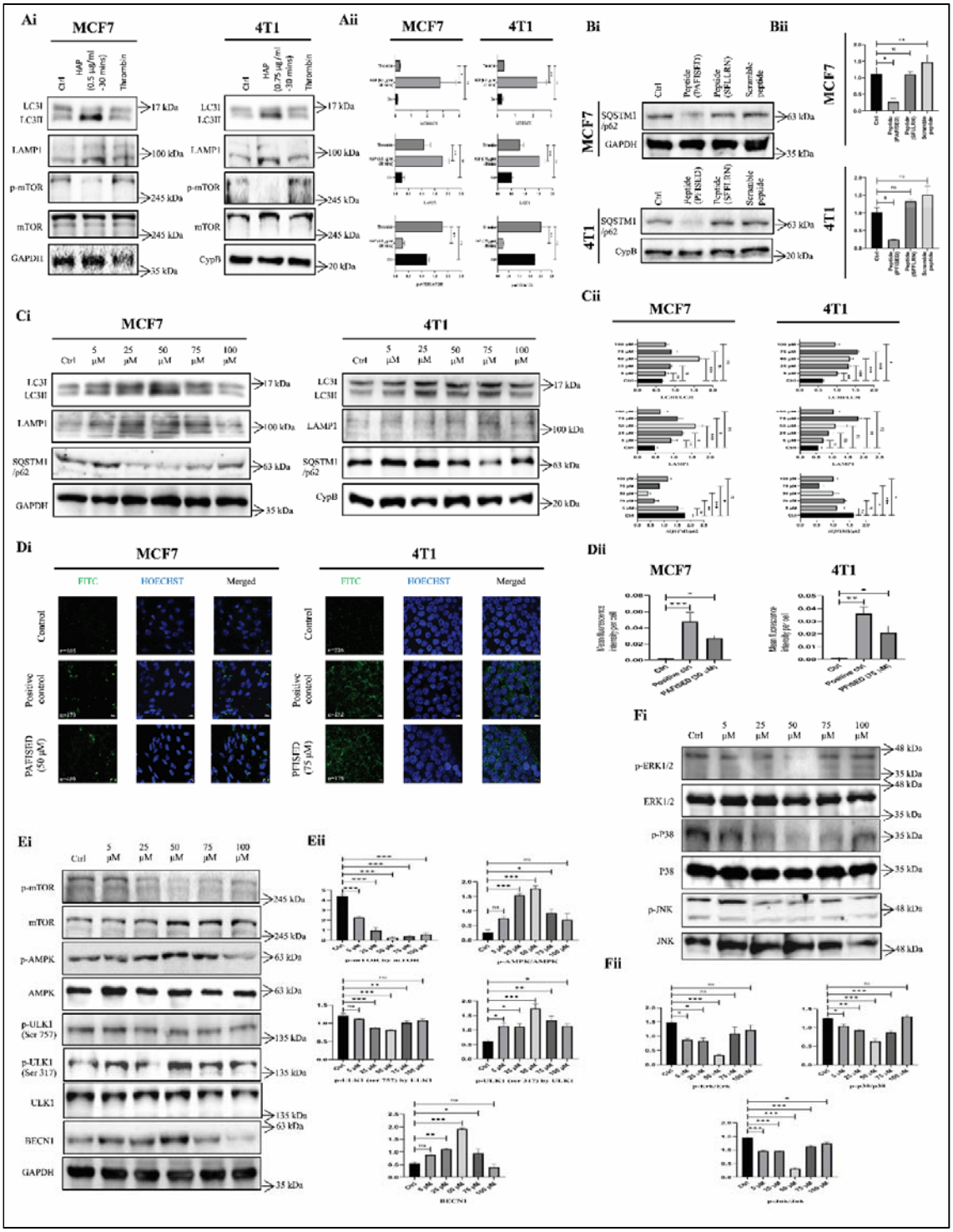
Ai
MCF7
4T1
Ctrl
HAP (0.5 μg/ml -30 mins)
Thrombin
LC3I
LC3II
LAMP1
p-mTOR
mTOR
GAPDH
CypB
17 kDa
100 kDa
245 kDa
35 kDa
20 kDa
Aii
Bi
Bii
SQSTM1 /p62
63 kDa
Ci
5 μM
25 μM
50 μM
75 μM
100 μM
Cii
Di
FITC
HOECHST
Merged
Control
Positive control
PATSFED (50 μM)
PTSFED (75 μM)
Dii
Ei
p-AMPK
AMPK
p-ULK1 (Ser 757)
p-ULK1 (Ser 317)
ULK1
BECN1
135 kDa
Eii
Fi
p-ERK1/2
ERK1/2
p-P38
P38
p-JNK
JNK
48 kDa
Fii

Figure 5

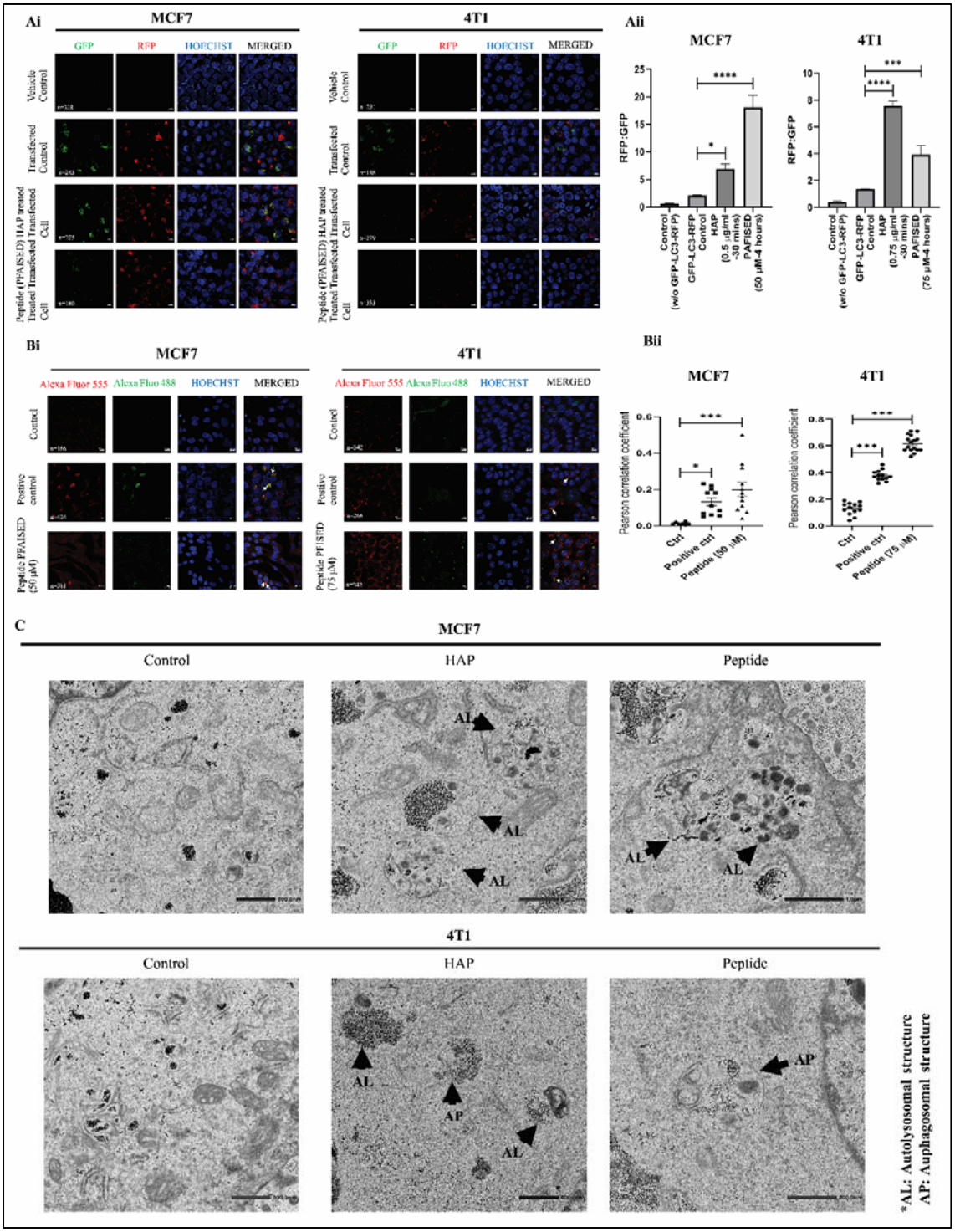
Ai
MCF7
4T1
GFP
RFP
HOECHST
MERGED
Vehicle Control
Transfected Control
Peptide (PEAISED) HAP treated Transfected Cell
Aii
RFP:GFP
Control (w/o GFP-LC3-RFP)
GFP-LC3-RFP
Control
HAP (0.5 μg/ml -30 mins)
PAFISED (50 μM-4 hours)
HAP (0.75 μg/ml -30 mins)
PAFISED (75 μM-4 hours)
Bi
Alexa Fluor 555
Alexa Fluo 488
Control
Positive control
Peptide PFAISED (50 μM)
Peptide PFISED (75 μM)
Bii
Pearson correlation coefficient
Ctrl
Positive ctrl
Peptide (50 μM)
Peptide (75 μM)
C
Control
HAP
Peptide
AL
AP
*AL: Autolysosomal structure
AP: Auphagosomal structure

Figure 6

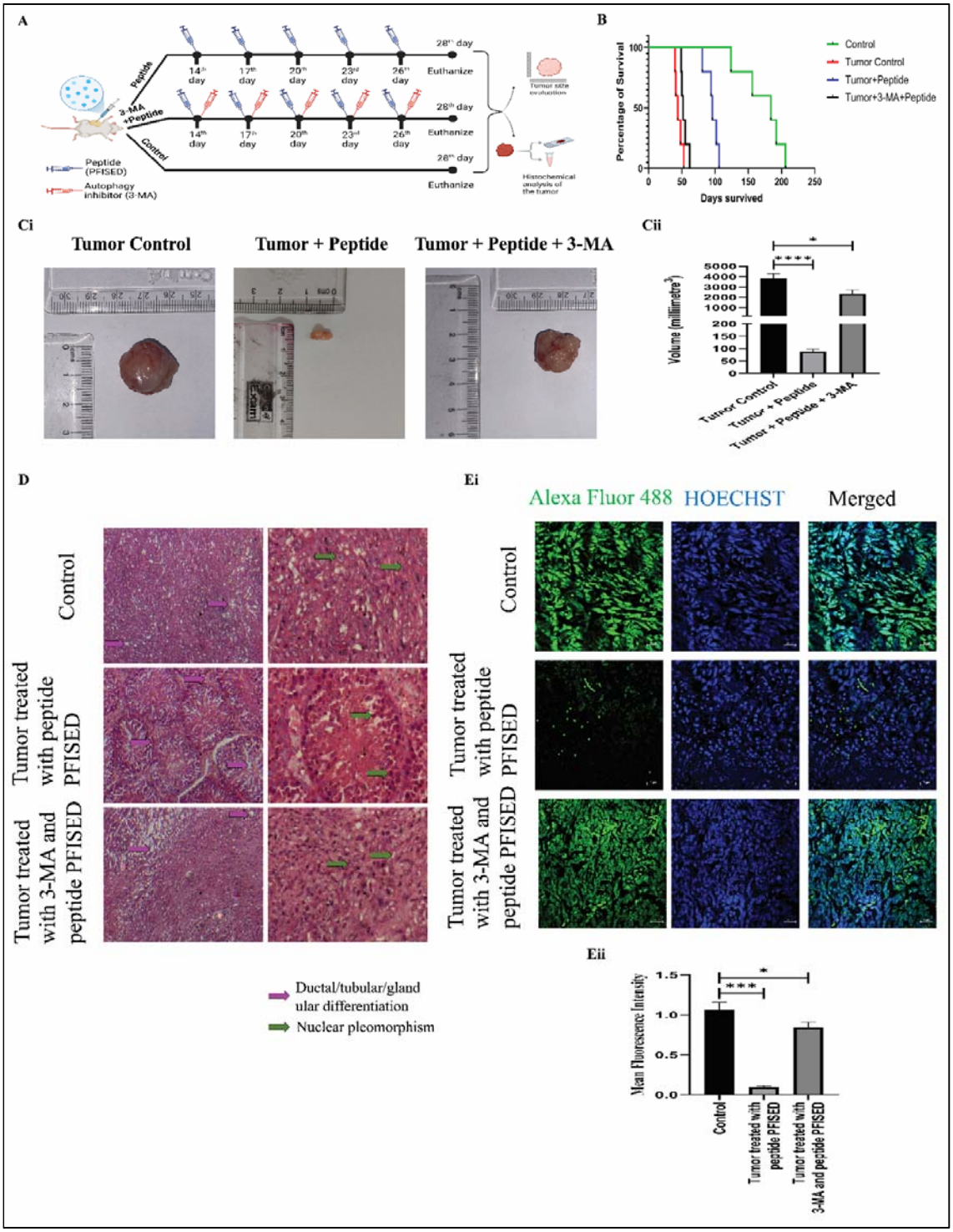
A
Peptide
3-MA +Peptide
Control
14th day
17th day
20th day
23rd day
26th day
28th day
Euthanize
Tumor size evaluation
Histochemical analysis of the tumor
Peptide (PFISED)
Autophagy inhibitor (3-MA)
B
Percentage of Survival
Days survived
Control
Tumor Control
Tumor+Peptide
Tumor+3-MA+Peptide
Ci
Tumor Control
Tumor + Peptide
Tumor + Peptide + 3-MA
Cii
Volume (millimetre³)
Tumor Control
Tumor + Peptide
Tumor + Peptide + 3-MA
D
Control
Tumor treated with peptide PFISED
Tumor treated with 3-MA and peptide PFISED
Ductal/tubular/glandular differentiation
Nuclear pleomorphism
Ei
Alexa Fluor 488
HOECHST
Merged
Control
Tumor treated with peptide PFISED
Tumor treated with 3-MA and peptide PFISED
Eii
Mean Fluorescence Intensity
Control
Tumor treated with peptide PFISED
Tumor treated with 3-MA and peptide PFISED

Figure 7

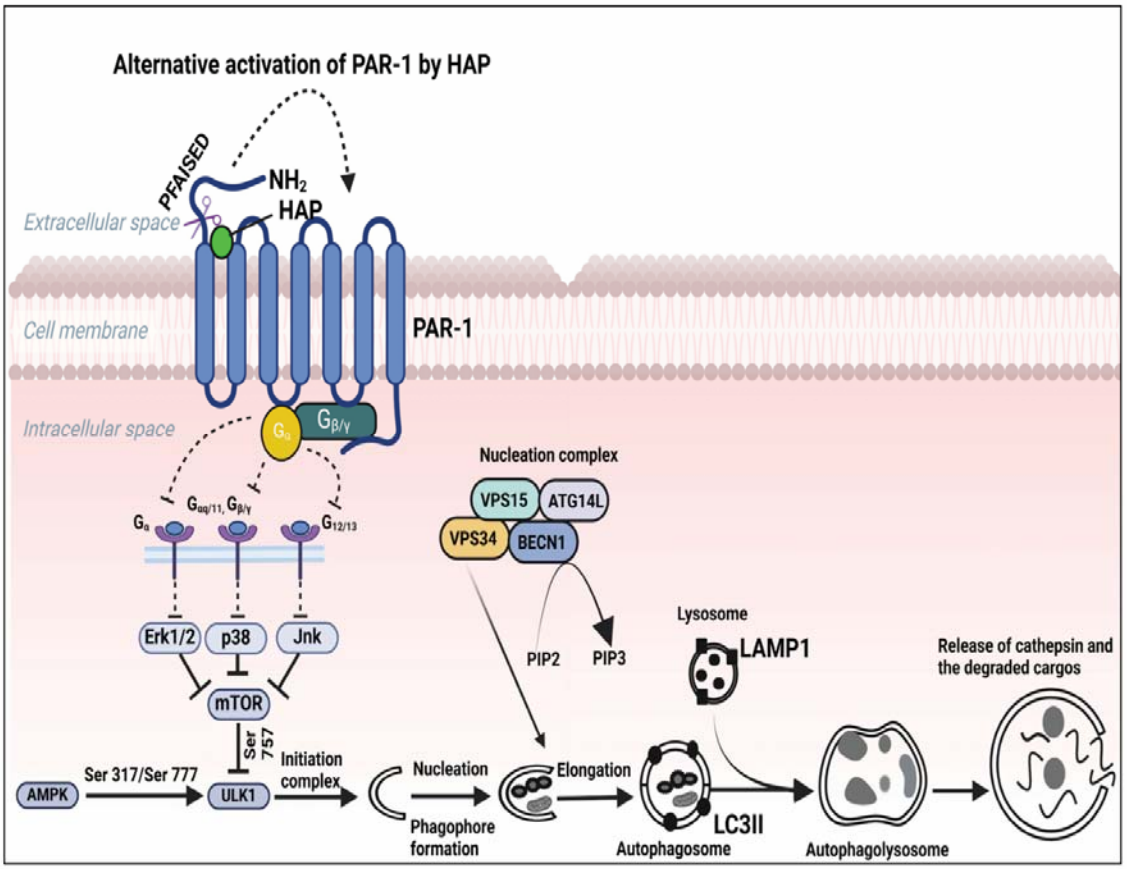
Alternative activation of PAR-1 by HAP
PFAISED
NH2
HAP
Extracellular space
Cell membrane
PAR-1
Intracellular space
Gα
Gβ/γ
Gα
Gαq/11, Gβ/γ
G12/13
Erk1/2
p38
Jnk
mTOR
Ser 757
AMPK
Ser 317/Ser 777
ULK1
Initiation complex
Nucleation complex
VPS15
ATG14L
VPS34
BECN1
PIP2
PIP3
Nucleation
Phagophore formation
Elongation
Lysosome
LAMP1
LC3II
Autophagosome
Autophagolysosome
Release of cathepsin and the degraded cargos